An accessible method to measure oxygen diffusion in cellular encapsulation devices for type 1 diabetes.

By: Kurtis Champion

Department of Chemical Engineering

McGill University

Montreal, Québec, Canada

Submitted April 2023

A thesis submitted to McGill University in partial fulfillment of the requirements of the degree of Master of Science in Chemical Engineering

Table of Contents

Abstract

Hydrogel-based cellular encapsulation is a technique used in many disciplines, such as 3D cell culture or therapies for a range of diseases, including cancer, acute liver disease, and diabetes. Several hydrogel-based pancreatic islet encapsulation devices are being developed and tested in clinical trials for type 1 diabetes to safely transplant islet grafts while avoiding immunosuppression. However, islet transplantation devices are often faced with oxygen limitations thereby impacting islet survival and function. Numerical models have been developed to predict oxygen concentration profiles in these systems to optimize device geometry. However, key model input parameters are often taken from literature instead of being measured experimentally. This can be problematic for parameters such as oxygen diffusivity in alginate, a natural polymer used in many islet encapsulation systems that shows significant lot-to-lot variability. In this work, a simple and accessible system was developed to measure the diffusion coefficient of alginate hydrogels, and then used to predict MIN6 cell behaviour. The system was validated by first verifying the surface boundary condition to determine if the system is diffusion driven, followed by measuring the oxygen diffusivity of water (37°C; $3.2 \times 10^{-5} \pm 0.5 \times 10^{-5}$ $cm^2 s^{-1}$). The oxygen diffusion coefficient for 3 formulations of alginate hydrogels were measured and compared. The difference in encapsulation materials showed significant changes in MIN6 cell viability at lower cell fractions (1.2 million cells/mL) but showed no significance at high cell fractions (10 million cells/mL). The trend between viability and cell fraction is consistent with theoretical trends using the Thiele modulus and the effectiveness factor. This work is expected to allow others other laboratories without specialized equipment to measure oxygen diffusion properties through various hydrogels for modeling and other quantitative purposes. Ultimately,

this research aims to help in the design of islet encapsulation and islet transplantation devices to expedite a treatment for type 1 diabetes.

Résumé

Plusieurs disciplines mettent en œuvre l'encapsulation de cellules dans des hydrogels, par exemple pour la culture cellulaire en 3D ou les thérapies pour une série de maladies, notamment le cancer, les maladies hépatiques aiguës et le diabète. Plusieurs dispositifs d'encapsulation d'îlots pancréatique à base d'hydrogel sont en cours de développement et testés dans le cadre d'essais cliniques afin de transplanter en toute sécurité des greffons d'îlots tout en évitant l'immunosuppression. Cependant, la performance de ces dispositifs d'encapsulation est souvent limitée par l'oxygénation des cellules ce qui réduit leur survie et leur fonction. Des modèles numériques ont été développés pour prédire les profils de concentration d'oxygène dans ces systèmes afin d'optimiser la géométrie des dispositifs. Cependant, les principaux paramètres d'entrée du modèle sont souvent pris dans la littérature au lieu d'être mesurés expérimentalement. Cela peut être problématique pour des paramètres tels que la diffusivité de l'oxygène dans l'alginate, un polymère naturel utilisé dans de nombreux systèmes d'encapsulation d'îlots de Langerhans, qui présente une variabilité importante d'un lot à l'autre. Dans ce travail, un système simple et accessible a été développé pour mesurer le coefficient de diffusion de l'oxygène dans des hydrogels d'alginate, puis utilisé pour prédire le comportement des cellules MIN6. Le système a été validé en vérifiant d'abord la condition limite de surface pour déterminer si le système est gouverné par la diffusion, puis en mesurant la diffusivité de l'oxygène dans l'eau (37°C ; $3.2 \times 10^{-5} \pm 0.5 \times 10^{-5}$ $cm^2 s^{-1}$). Le coefficient de diffusion de l'oxygène pour 3 formulations d'hydrogels d'alginate a été mesuré et comparé. Un effet significatif des différentes compositions d'alginate sur la viabilité de cellules bêta MIN6 a été identifié, mais seulement dans des conditions où la concentration cellulaire était faible (1.2 millions de cellules par mL) et non pas dans des conditions de concentration cellulaire élevée (10 millions de cellules par mL). La

tendance entre la viabilité et la fraction cellulaire est cohérente avec les tendances théoriques utilisant le module de Thiele et le facteur d'efficacité. Ce travail devrait permettre à d'autres laboratoires ne disposant pas d'installations spécialisées de mesurer les propriétés de diffusion de l'oxygène à travers divers hydrogels à des fins de modélisation et d'autres objectifs quantitatifs. En fin de compte, cette recherche vise à contribuer à la conception de dispositifs d'encapsulation et de transplantation d'îlots afin d'accélérer le traitement du diabète de type 1.

Acknowledgement

I would first like to say thank you to both my supervisors Dr. Corinne Hoesli and Dr. Richard Leask. Without your guidance this work would have been impossible. All the time, impromptu meetings and chats, and help is what made this project possible. With your guidance, I am now able to think much more critically about almost everything and feel much more rounded as a scientist.

Thank you to the support from all of the funding agencies which made this project possible including: 2019 Stem Cell Network Fueling, Biotechnology Partnerships grant in partnership with Aspect Biosystems, Natural Sciences and Engineering Research Council (NSERC) Discovery (RGPIN-2020-05877 and RGPIN-2018-06161), the Vadasz Scholar award, the funding provided by McGill University from the McGill Engineering Doctoral Award (MEDA), as well as the funding from agencies like the Fonds de recherche du Québec (FRQNT). Thank Aspect Biosystems for the support at the beginning of my project. I would also like to thank Jesse Ehrlick and André Tremblay for coordinating my MedTech internship and its associated funding agencies (NSERC CREATE and BioTalent). Id like to acknowledge the building staff who helped make my project possible, including Louise Miller-Aspin, Beata Kaatori, Lisa Volpato, Frank Caporuscio, and Austin Duffett. Thank you for the administrative help to provide a path to follow for my complicated degree choices or helping me build and maintain equipment for my experiments.

I would like to thank all of the people who helped me make this project possible, including Lisa Danielczak, Laurier Gauvin, Jonathan Brassard, Florent Lemaire, Dongjin Shin, and many others. Your help in brainstorming solutions to research problems, collecting vital research data, or simply being there to ensure me that this is just part of the process is what made this work

possible. I would also like to thank Mohamed Elkhodiry who supervised my first summer internship in the Hoesli lab and made me interested in research.

Finally, I would like to thank my family for the support and thanks to my partner Aly who was there for me every step of the way.

List of Figures

List of Tables

List of Abbreviations

β cell – Beta cell

1D – One-dimensional

C_0 – Initial concentration

$CaCO_3$ - Calcium carbonate

$CaCl_2$ - Calcium chloride

CFD – Computational fluid dynamics

CGM – Continuous Glucose Monitor

CO_2 – Carbon dioxide

DMEM – Dubelcco's Modified Eagle Medium

Em - Emission

Ex - Excitation

FBS – Fetal Bovine Serum

FRQNT - Fonds de recherche du Québec

GDL – Glucono Delta-Lactone

gluc – Glucose

H^+ - Hydrogen ion

IEQ - Islet Equivalent

(IL)1β – Interleukin

(INF)γ – Interferon

K_m – Michaelis-Menten coefficient

M/G – Ratio of mannuronic acid to guluronic acid

MIN6 – Mouse Insulinoma 6 cell line

N_2 – Nitrogen

NSERC - Natural Sciences and Engineering Research Council

O_2 - Oxygen

OCR – Oxygen Consumption Rate

PEG – Poly-ethylene glycol

Pe - Peclet number

pO_2 – Oxygen partial pressure

RAMQ - Régie de l'Assurance Maladie du Québec

T1D – Type 1 Diabetes

(TNF)α – Tumor Necrosis Factor

Contribution of Authors

The manuscript-based thesis that follows consists of an article to be submitted to publication is a peer-reviewed journal. I am the primary author of this work and this thesis.

K.S. Champion, L. Gauvin, J. Brossard, R.L. Leask, C.A. Hoesli, An accessible method to measure oxygen diffusion in cellular encapsulation devices for type 1 diabetes., (2023).

I performed all of the experiments, writing, and work in this manuscript, except for a few experimental replicates for Fig. 3-8 performed by second author and third author Laurier Gauvin (undergraduate researcher) and Lisa Danielczak (technician), whom I supervised. I analyzed all of the results, as well as prepared and edited the manuscript for submission. The second and third authors Laurier Gauvin & Lisa Danielczak were responsible in helping with data collection, experiment planning, and cell culture. The fourth author Jonathan Brassard (PhD student) helped in the conceptualization of the experiments during development. The authors Corinne Hoesli and Richard Leask were responsible for supervising the project, guidance, editing the manuscript, and acquiring the funding necessary for the work to transpire.

1 Chapter 1: Introduction

1.1 Overview

Type 1 diabetes is a lifelong autoimmune disease where patients must regulate their own insulin ang glucose levels. The reason this disease leads to loss of glucose regulation is because of beta cell destruction [1,2]. Beta cells are part of cell clusters known as islets of Langerhans natively found in the pancreas and regulate blood-glucose levels in the body by producing insulin [3]. Islet transplantation is seen as one of the most promising treatments to type 1 diabetes. Currently, it has been shown to reverse diabetes in mice [4,5], has been carried through in phase 3 trials for humans [6], and has a dedicated clinic in Québec to allow for access to the treatment provincially [7]. Despite the promise for this therapy, one of the major problem with islet transplantation as a commercial diabetes treatment is the large number of islets needed to account for early cell necrosis, which is commonly associated with insufficient oxygen (hypoxia) and lack of vascularization [8,9]. This problem is worsened by the high demand for this treatment and lack of donors. Even for those who do get access to the treatment, islet transplantation relies on the use of immunosuppressants to stop the hosts immune system from attacking the newly transplanted islets. Immunosuppressants carry their own burdens such as increased chances of cancer, infection, and reduced immunity.

Another more experimental method in stopping islet death is islet encapsulation. Encapsulation uses the size exclusion properties of hydrogels like alginate to allow nutrients and small molecules like insulin to pass through to the islet, but block macrophages or autoimmune antibodies to come in contact with the cell aggregate [10,11]. Despite encapsulation having the ability to supress cell death associated with an autoimmune response, problems like hypoxia or nutrient mass transfer are exacerbated by encapsulation and can adversely affect islet viability

[9]. Another major factor that increases hypoxia is the large cell density needed for a human-scale device. The most conventional encapsulation techniques are making microbeads and macroencapsulation devices. Ideally the transplantation device would be as small as possible while adequate oxygenation which remains a challenge [12].

Due to the high demand of islets, numerical modelling can be a useful tool for early device prototyping since not as many islets are necessary for research and development purposes. A numerical model with validated inputs could be beneficial both in understanding the viability of islet encapsulation technologies, as well as optimizing the many different geometries and configurations of medical devices without requiring islets. Ideally, to make numerical models as accurate as possible, they should have all of their inputs experimentally validated.

Some of the parameters that are critical for oxygen mass transfer numerical modelling like the oxygen diffusion coefficient are not simple to measure and requires specialized equipment. Currently, the methods to measure oxygen diffusion in hydrogels could involve the use of optical probes to monitor change in fluorescence over time that is linked to oxygen diffusion [13,14]. Other techniques involve the use of a stirred tank apparatus or is measured indirectly alongside the oxygen consumption kinetics of a certain cellular system as a fitting variable [15,16]. As a result of the challenge in measuring the diffusivity hydrogels may be assumed to have diffusivity that is proportional to their porosity (ex: 98% water) or to that of another hydrogel formulation. Since hydrogels are viscoelastic materials, there properties can vary greatly from one formulation to another, making it even more important to measure the diffusion coefficient experimentally. One of the main objectives of this work is to develop a more accessible method to measure this parameter with a more conventional laboratory equipment.

1.2 Objectives

This work aims to investigate the effects of alginate-based encapsulation materials on cell viability and predict cellular behaviour using an experimentally validated numerical model for oxygen diffusion. The main objectives of this work are to (1) develop a simple and more accessible way to measure the oxygen diffusion of liquids and hydrogels, (2) experimentally measure the oxygen diffusion of alginate-based encapsulation materials, (3) use the measured parameters to predict the cellular behaviour of mouse insulinoma cells (MIN6) using a numerical model.

2 Chapter 2: Background and Literature Review

2.1 Type 1 diabetes and islet encapsulation

Type 1 diabetes (T1D) is a lifelong autoimmune disease that affects 15 out of 100,000 people globally and is usually diagnosed before the age of 20 [1,2]. The insulin producing β cells in cell clusters known as Islets of Langerhans, are destroyed in an autoimmune response [11,17]. Islets regulate glucose in the body primarily through the release of insulin and are natively found in the pancreas. In general, non-diabetic patients have a blood-glucose range from 3 mM to 15 mM but is usually between 4-6mM [18–20]. Islets are composed of multiple different cell types, including α, β, γ, and pancreatic polypeptide cells [17]. The β cells are the cells primarily involved in maintaining normoglycemia (Fig. 2-1) and despite only composing 1-2% of the cells in the pancreas, they receive 20% of its blood flow [17].

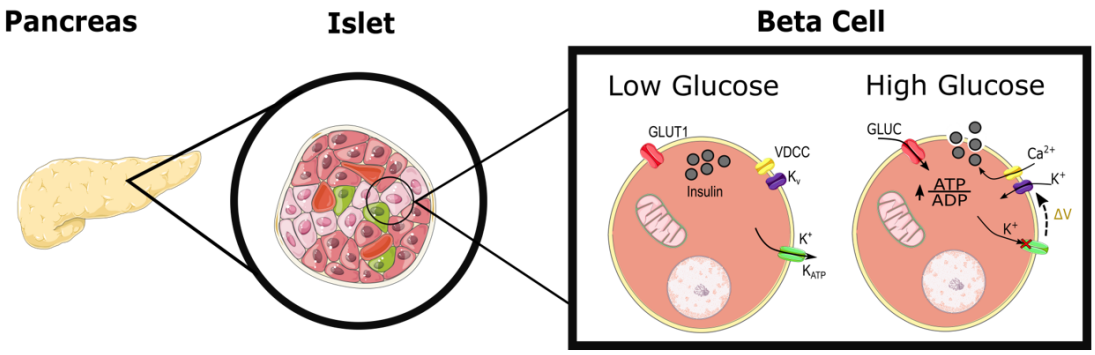

Fig. 2-1 β cell glucose regulation (adapted from [3])

Note that the β cell regulate glucose levels by first sensing glucose, and then releasing an appropriate amount of insulin globules determined by calcium influx and potassium efflux [3].

As of today, T1D patients must regulate their insulin levels exogenously either manually through consistent monitoring with or without a continuous glucose monitoring device (CGM), or automatically with an insulin pump [21]. However, exogenous insulin delivery methods will never be as effective at regulating glucose as native islets [21,22]. Even in automatic systems like an insulin pump with a CGM, the insulin-glucose relationship is hard to control. This is primarily due to the significant lag time between when the insulin is administered and when it takes effect [21]. As a result, T1D patients still have a shortened lifespan due to chronic glucose dysregulation [11].

Islet transplantation is a cellular therapy where islets are transplanted in T1D patients and when successful it has shown to have much better control on glucose levels than exogenous methods such as insulin injections. Islet transplantation provides better regulation because they control glucose levels continuously and on a cellular level using osmolarity as shown in Fig. 2-1. Unfortunately, islet transplantation alone is not a long-term solution as the immune system will still attack the newly implanted islets, or they will die as a result of disrupted vascularization

when removed from the transplant donor [9,22]. To circumvent graft rejection, patients who undergo islet transplantation are currently placed on life-long immunosuppressive drugs to prevent an autoimmune response. However, immunosuppressive treatments can have negative side effects like increased chance of infection or cancer, making them less attractive as a final solution [23,24]. Another more experimental option to avoid graft rejection is islet encapsulation. In islet encapsulation, a hydrogel is used to create size exclusion membrane around the islet which theoretically allows free entry and exit of nutrients, glucose, insulin, etc. but has pores too small for larger entities like autoimmune antibodies or immune cells (Fig. 2-2) [10,11,25].

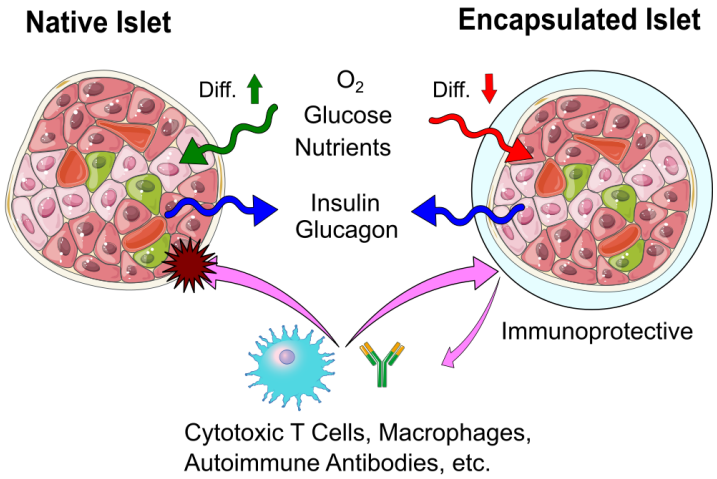

Fig. 2-2 Islet encapsulation principle (adapted from [10])

The major limitation with islet encapsulation is the number of islets required to cure T1D. Islet isolation from a human pancreas can yield 300,000 to 600,000 islets [26], while roughly 10,000 islets equivalent per kg (IEQ/kg) are needed for islet transplantation (~600,000 islets for a 60kg human) [27]. While there are many issues currently limiting access to clinical islet transplantation, some important ones are: the scarcity of islets available, and the high number of islets needed for transplantation [28]. These limitations also highlight that islet encapsulation as a

cellular therapy is still in development. However, solutions to these limitations are currently in development alongside islet transplantation. One promising solution is the use of islet derived stem cells (iPSC). iPSCs represent a virtually unlimited source of cells for transplantation and could solve some of the major current obstacles with islet transplantation [29].

Islets are encapsulated in many ways. The two major categories are macroencapsulation and microencapsulation. Microencapsulation consists of individually encapsulating each islet in the form of beads, while macroencapsulation can have multiple islets encapsulated in a single device.

Microencapsulation generally provides better oxygen and nutrient transport due to the smaller diffusion layer around the islet. However, macroencapsulation can be optimized into many different geometries such as: fibers, pouches, sheets, internal perfusion devices, etc. Macroencapsulation also has the advantage of being a retrievable post-transplantation, which is not the case with microencapsulation [30]. The most common hydrogel used for islet encapsulation in literature is alginate, attributed to its low cost, tunable properties, and its immunoprotective capabilities. [30–33]. Islets can also be encapsulated in different materials like poly-ethylene glycol (PEG), so long that the porosity of the material allows for proper nutrient and oxygen diffusion while also being immunoprotective [34]. The advantage in using a synthetic material like PEG instead of alginate for encapsulation is that the material properties have less variability. Nevertheless, alginate remains one of the most used substances for islet encapsulation since it has been well-studied, is a mature technology, and comes from a low-cost renewable source (brown algae) [32,35,36]. Alginate encapsulation has shown to provide long-term immunoprotection in primates, and has progressed to human clinical trials [32,37].

2.2 Islet oxygenation and hypoxia

During islet transplantation, an excess of islets are needed to compensate for the cell necrosis, particularly at the center of the islet [38]. The primary reason for this is the lack of nutrients and oxygen associated with the removal of native islet microvasculature [9]. As shown in Fig. 2-3a, islets in the native pancreas have blood vessels that serve to deliver nutrients (oxygen, glucose, etc.) to the β cells at the center of the islet resulting in high cell viability [9]. Fig. 2-3b and Fig. 2-3c illustrate how after islet isolation and encapsulation this microvasculature is disrupted, resulting in reduced nutrient supply [9]. Cells at the center of an encapsulated islet depend solely on diffusion for nutrients and are most susceptible to cell necrosis [39].

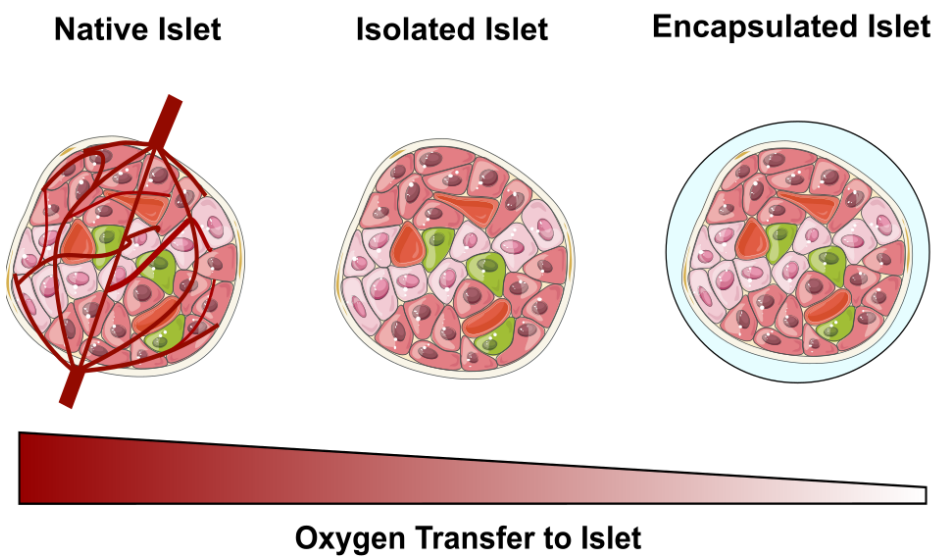

Fig. 2-3 Islet nutrient supply in (a) the pancreas (b) after isolation, and (c) after encapsulation (adapted from [9])

One of the major sources of cell necrosis in encapsulated islets is lack of oxygen and nutrients. In general, the partial pressure of oxygen (pO_2) in the body ranges from 0% to 14% O_2 (0 to 100 mmHg) as shown in Fig. 2-4 [40]. The most common islet transplantation site is the liver,

specifically the portal vein [41]. Although, there are many preclinical or clinical transplantation sites in development. Some of these alternative sites are the subrenal space in the kidney [42], which according to Fig. 2-4, has an oxygen tension of 7% O_2 (~54 mmHg) [43] or the omentum as it is known for being a highly oxygen and nutrient rich location [44].

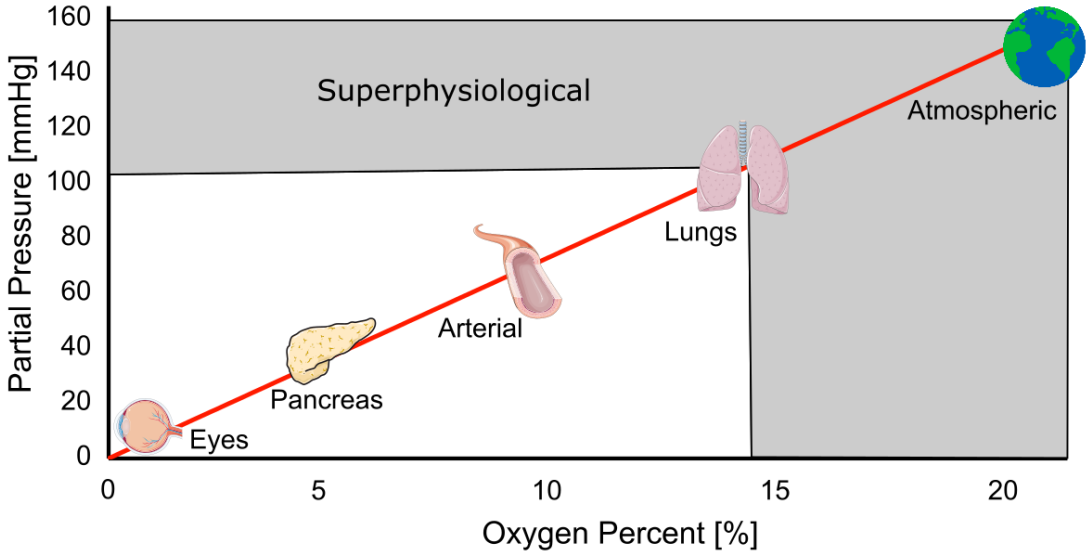

Fig. 2-4 Partial pressure of oxygen for different organs in the human body (adapted from [40])

Hypoxia and cell necrosis in islets is commonly reported when the pO_2 drops below 0.1mmHg [19,39]. Nevertheless, many sources report that insulin secretion begins to reduce at partial pressures below 5.1 mmHg (~0.6% O_2) [39,45]. In fact, other sources suggest this value to be even higher, showing reduced insulin release at pO_2's as high as 5% (38mmHg) [46]. Despite the body having a maximum oxygen tension of about 100 mmHg, islets can survive supraphysiological conditions with oxygen tensions as high as 75% O_2 (570 mmHg) without significant loss of viability [47].

The proper oxygenation of human scale islets remains a challenge. Current estimates suggest that macroencapsulation devices would have to be very large to properly oxygenate a human scale

number of islets in vivo, some estimate the size to be a flat screen tv (in 2016), others estimate it would be ~1000 IEQ/cm^2 or a 600 cm^2 sheet for 600,000 islets with support from vasculature [12,48]. Nevertheless, islet encapsulation is a promising cell therapy as it can provide glucose regulation, and immunoprotection for islets.

2.3 Other factors affecting survival and their effect on oxygenation

While alginate itself creates an oxygen diffusion barrier, there are other factors that will impact oxygen availability to the graft, as well as graft survival and function. One example of these factors is the inflammation that occurs after transplantation. The damaged tissue may release cytokines which recruit immune cells such as monocytes and macrophages [49,50]. Moreover, a hydrogel like alginate can degrade over time [51], and may trigger a foreign body response or contribute to inflammation because of its formulation (mechanical properties, biocompatibility, pore size, topography, cell fraction, if it releases molecules like endotoxins, etc.) [52–54].

One example of how formulation can contribute to inflammation is the production of nitric oxide (NO) and reactive oxygen species (ROS) [53,55]. These molecules are produced by the islets as a result of inflammation after transplantation, both NO and ROS pose oxidative stress on the islets and contribute to loss of islet function in high enough concentrations [53,55]. Moreover, ROS and NO are small enough to permeate through hydrogels used for encapsulation [53]. If many islets are transplanted close by, this could lead to oxidative stress as the encapsulation material cannot protect the cells from the large amounts of NO and ROS. However, due to the short half lives of ROS and NO, having lower cell fractions in the alginate formulation may mitigate this issue as these molecules will not be accumulate in sufficiently high concentrations to damage the islets [53].

Another example of how inflammation is an important consideration for hydrogel formulation is the effect of cytokines. While encapsulation theoretically prevents contact between the graft and components of the immune system such as T cells or antibodies, the pore sizes of the hydrogel typically allow permeation of cytokines. Among these cytokines, tumor necrosis factor (TNF)α, interleukin (IL)1β, and interferon (INF)γ have all been shown to affect islet survival or function [49,50,55–58]. While alginate alone has had good success [4,59], newer encapsulation materials or different alginate composites have been developed to perform with improved biodegradation and biocompatibility [58,60–62]. However, any encapsulation material will still add an additional oxygen diffusion layer, thus finding an ideal material and method for long-term graft success while also providing proper immunoprotection and proper islet oxygenation remains a challenge.

The foreign body response that occurs after transplanting the encapsulation material can lead to fibrosis, and can cause immune cells (myofibroblasts, macrophages, etc.) to accumulate onto the device surface impacting islet survival and oxygenation [52,63,64]. The immune cells which were recruited to the surface of the graft may release harmful cytokines that would affect graft survival [49,50,55]. Moreover, the fibrotic layer consumes oxygen and acts as yet another oxygen diffusion barrier for the islets. Often, these fibrotic layers do not resorb and continue to recruit more immune cells to the surface of the graft with time. This continuous cell recruitment then exacerbates oxygen availability as more cells are consuming and preventing oxygen from reaching the core of the islet [52,64]. In this vicious cycle, the resulting hypoxia may cause islet cytokine release which would continue to promote even more immune cell recruitment, again reducing oxygen availability. Islet oxygenation modeling should not only consider graft oxygen demand but also these other factors, especially if fibrotic layers consume oxygen and create a

secondary diffusion barrier; other work has considered fibrosis in modelling before ([65] as an example). However, the effect of fibrosis in islet oxygenation modelling, the relationship between cytokines and hypoxia, and downstream adaptive responses remain outside the scope of this thesis.

2.4 Classic modelling theory applied to the oxygenation of islets

A lot of work has gone into making representative oxygen models for islets, primarily due to their scarcity and high demand for transplantation [27,28,39]. Oxygen consumption kinetics for islets has been thoroughly investigated [18,39,66,67]. Despite these efforts, rigorous experimental validation of key modelling parameters like the diffusion coefficient remains a challenge.

Classic transport phenomena theory can also apply to a system like an encapsulation device. In general, mass transport follows the advection-diffusion equation:

$$\frac{\partial C}{\partial t} + u\nabla \mathrm{C} - \mathrm{D}\nabla^2 \mathrm{C} = \mathrm{R}$$

C (concentration), t (time), u (velocity), D (diffusion coefficient), R (reaction), ∇ (δC/δx, δC/δy, δC/δz)

Where in this case, the complexity of an islet is reduced to a single entity that consumes oxygen in the reaction term (R). If there are more cells in a confined space, the cellular density increases, the consumption of oxygen will increase, and the reaction rate increases. Similarly, if one cell type consumes oxygen more rapidly than another, then for the same cell density, the overall oxygen consumption will increase, and so will oxygen consumption reaction rate. In general, the oxygen consumption rate (OCR) of a cell is in units $mol \bullet m^{-3}s^{-1}$, the kinetics can be simplified to a 0^{th} order reaction if the Michaelis-Menten coefficient (K_m) of the system is much smaller than

the surface concentration (C_0). For example, in a system where the cells are in an incubator in a thin diffusion layer of media with atmospheric oxygen levels, this will be true as $C_0 >> K_m$ (160mmHg >> 0.44 mmHg)[19,68]. However, if the cells are in vivo in an oxygen limiting environment, or if there is a larger diffusion layer before the surface of the cells, this may no longer be true, and a refined model is needed.

The most common model for islet oxygenation is Fick's law with Michaelis-Menten kinetics [39,68–70]. In general, the time dependent term is neglected since type 1 diabetes is a lifelong disease, and most insulin-glucose modulating experiments take place over days or weeks making this a reasonable assumption. Many different models have been made to capture the oxygen consumption kinetics of islets [27,39]. The simplified differential equation would be as follows:

$$D\nabla^2 C = R$$

Where the reaction R follows Michaelis-Menten kinetics. Since only the cells are consuming oxygen and do not compose the entire volume of the hydrogel, the reaction term is often weighted by the cell fraction or occupied space (ε) [68]. The overall equation would be:

$$D\nabla^2 C = (1-\varepsilon)\left(V_{max}\frac{C}{C+K_m}\right)$$

Often times, the reaction term is simplified to 0^{th} order kinetics and appears as $(1-\varepsilon)(V_{max})$ since $C >> K_m$ [68].

Other modelling approaches prefer to use the solubility term to convert the equation into partial pressure[39,69,70]. This conversion done by using the following relationship:

$$C = \alpha P$$

Where α is the solubility (constant) and P is the partial pressure of oxygen. As a result, the differential equation would be written as follows:

$$D\alpha\nabla^2 P = R$$

This approach is preferred by many since the partial pressure of oxygen is the conventional unit in islet cell biology.

One particularly interesting model is one that captures the effect of cell necrosis in hypoxic conditions ($pO_2 < 0.1$mmHg) [19,39,70], and the effect of glucose levels on islet oxygen consumption. Higher blood-glucose levels will stimulate more insulin production and release thereby indirectly increasing oxygen consumption in the islet due to increased metabolic activity [18].

The reaction term for this model is represented in the following equation [18]:

$$R = R_{max,O_2}\phi_{scale}\left(\phi_{base} + \phi_{metabolic}\frac{C_{gluc}^n}{C_{gluc}^n + K_{m,gluc}^n}\right)\frac{C_{O_2}}{C_{O_2}+K_{m,O_2}}\delta(C_{O_2} > C_{cr})$$

The reaction kinetics for glucose (gluc) and oxygen (O_2) consumption follow Hill and Michaelis-Menten kinetics respectively. The correlation uses adjustment factors to create a better fit for the model, these include: $\phi_{metabolic}$ which accounts for the metabolic activity of the islet, ϕ_{base} which is the base oxygen consumption rate, and ϕ_{scale} which serves to scale the model so that oxygen consumption increases by 70% when glucose levels rise from 3 mM to 15 mM [18,19]. Furthermore, the model uses a Heaviside function that serves to eliminate any oxygen consumption when oxygen concentrations drop below those associated with cell necrosis (C_{cr};

0.1mmHg; $1.65x10^{-4}$ M). Finally, R_{max} represents the maximum oxygen consumption rate (OCR) [18,19,39,71].

The limitations of these models are that they are commonly employed on single islet models and lack a thorough experimental validation of the modelling parameters. Moreover, many oxygen models neglect advection due to their microscopic nature, but for macroencapsulation devices this may lead to model inconsistencies, especially in a scenario with internal perfusion where flowrate can change oxygen availability throughout the device.

2.5 The Thiele modulus and effectiveness factor applied to islet oxygenation

The objective of this work is to quickly optimize an encapsulation device in order to improves cell viability and function. One way this can be done is by analysing the system using the Thiele modulus and effectiveness factor. The Thiele modulus (φ) describes the ratio between the reaction rate and the diffusion rate:

$$\varphi = \frac{reaction\ rate}{diffusion\ rate}$$

It is a dimensionless number that essentially describes how well the system is being oxygenated. For low values of the Thiele modulus, there is an abundance of oxygen for the given cells and the oxygen transport is not limited by diffusion. At very high values of the Thiele modulus, the oxygen cannot diffuse fast enough to meet the oxygen consumption demand of the cells. This phenomenon is also captured in the effectiveness factor (η): for an effectiveness factor of 1, all the cells will have adequate oxygenation, however as the system becomes more diffusion limited (φ↑) the effectiveness factor decreases toward 0. When the effectiveness factor approaches 0, the

oxygen cannot be replenished fast enough in the material to meet the oxygen demand of the cells.

Adequate cell oxygenation then depends greatly on the diffusion properties of the material, provided that the cell fraction is low enough to have a high effectiveness ($\eta \geq 0.9$). The diffusion coefficient (D) in the advection-diffusion equation describes how well oxygen moves through the hydrogel without velocity.

2.6 The oxygen diffusion coefficient of encapsulation materials

While recognizing there are many factors that can affect the behaviour of cells, such as the glucose concentration, necrotic cell signaling, etc. this work will focus on the effect of a couple of major methods used in encapsulation devices. This work tries to isolate the effect of the diffusion coefficient and the cell fraction on cell viability and explain its connection to classic mass transport theory.

In current literature, reporting of all critical oxygenation parameters for cell culture and reproducibility remains a challenge [72]. This challenge is also true for numerical modelling, likely due to resources and ability to experimentally measure parameters like the oxygen diffusion coefficient. This work aims at developing a simple way to measure the oxygen diffusion coefficient for hydrogels to eliminate the generalizations about the diffusion of hydrogels and assess the effect of diffusivity on cell viability.

The porosity of hydrogels like alginate can vary significantly based on the material properties like the molecular weight and ratio of mannuronic acid (M) and guluronic acid (G), hereon

referred to as the M/G ratio. Alginate strands generally follow a $(M\text{-}M\text{-}G\text{-}G\text{-}M\text{-}M)_n$ structure which resembles an egg box structure when cross-linked.

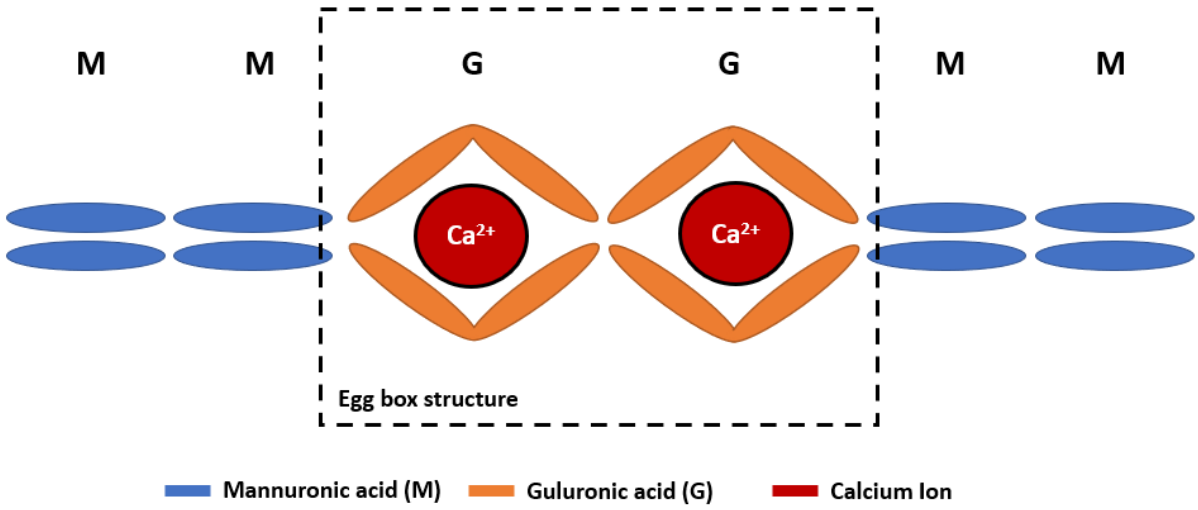

Fig. 2-5 Alginate egg box structure (adapted from [73])

The crosslinking ion (like Ca^{2+}) sits in the "egg" position located between the two G molecules as shown in Fig. 2-5. Therefore, alginates that are more G rich tend to be stronger with a higher Young's modulus [74]. They also tend to be less porous since G rich gels will be physically more crosslinked than M rich gels. The alginate porosity also depends on the molecular weight of the alginate strands [75]. Current theory suggests that cross-linked alginate with a low M/G ratio and low molecular weight will result in a less porous alginate matrix. Theoretically, a lower M/G ratio and smaller pores physically inhibit diffusion, while a smaller molecular weights lead more organized structures which makes the hydrogel less diffusive [75]. Current values in literature for the oxygen diffusion coefficient in alginate hydrogel formulations can range anywhere from $0.7\text{x}10^{-5}$ to $2.6\text{x}10^{-5}$ cm^2s^{-1} [18,76–78]. These diffusion coefficient values are on the order of magnitude of water, which has literature values mostly ranging from $2.9\text{-}3.3\text{x}10^{-5}$ cm^2s^{-1}

[18,72,79–81]. The porosity may have an effect on the oxygen diffusion coefficient of alginate, which is something that will be investigated in this work. In general, there are two different types of gelation, external gelation and internal gelation [82]. An example of external gelation is adding the alginate into a solution of calcium salt, such as $CaCl_2$ [83]. In this scenario, the calcium ions from $CaCl_2$ freely dissociate and cause alginate cross linking.

Internal gelation can be done in many ways, and in some cases, can happen slow enough to be casted into a mold before gelling completely. One method that accomplishes this with glucono-delta-lactone (GDL) and calcium carbonate ($CaCO_3$) [82,84]. In this method, alginate is cross-linked slowly by Ca^{2+} ions being released through a hydrolytic reaction with GDL and $CaCO_3$. By-products of this reaction is the release of H^+ ions and CO_2 gas [82,85]. Another method of internal gelation is the use of acetic acid to decrease the pH of a stirred emulsification containing $CaCO_3$. The pH drop from acetic acid causes Ca^{2+} to be released from $CaCO_3$ leading to alginate gelation [86].

Another material property of the material that surely influences the oxygen diffusion coefficient is the viscosity. The Stokes-Einstein relationship defines the theoretical diffusion coefficient as [87]:

$$D = \frac{k_B T}{3\pi\eta R_H}$$

D (diffusion coefficient); k_B (Boltzmann constant); T (temperature); η (viscosity); R_H (hydrodynamic radius)

This diffusion coefficient corresponds to a particle with a hydrodynamic radius of R_H. More importantly in the context of this work, the diffusion coefficient is inversely proportional to the viscosity of the fluid (η) which is assumed constant. Therefore, more viscous alginates may be

less diffusive according to this theory. However, it is difficult to measure the viscosity of cross-linked alginate because they are highly viscoelastic and non-linear, which is why in this work we we intend to investigate how the diffusion coefficient is affected by variables like the complex viscosity or complex modulus of elasticity (storage and loss modulus).

A key modelling parameter like the oxygen diffusion coefficient should be measured experimentally, especially for a hydrogel like alginate since it has material properties that can vary greatly and influence diffusivity. To improve model reliability, more work needs to go into properly measuring oxygen diffusivity and its relationship with the material properties of the encapsulation material. Ultimately, this may lead to a more accurate numerical model and easier rapid prototyping of islet transplantation devices.

The diffusion coefficient of encapsulation materials is a clinically relevant parameter which needs optimization. A more diffusive material could translate to an immunoprotective medical device that is smaller, requires less donated islets, and still delivers a therapeutic dose, however, if it is more diffusive this could also lead to less immunoprotection. Ideally, the diffusion coefficient of the material will be optimized and/or chosen to meet the specifications of the medical device.

2.7 Current methods to measure the oxygen diffusion coefficient of hydrogels

For modelling purposes, the oxygen diffusion coefficient can be estimated using known values of similar materials/ formulations or based on the porosity (ex: 98% water). However, few studies investigate the experimental oxygen diffusivity in the hydrogels used in encapsulation or modelling.

Most methods to quantify oxygen diffusivity in hydrogels rely on setups which measures the change in oxygen overtime after a step change. This can be difficult to achieve due to the high-water content of hydrogels, and hence any evaporation in small-scale or thin-film approaches can be problematic. One simple and accessible approach to measure oxygen diffusivity is to create alginate beads and deoxygenate them. After adding these beads into a stirred tank apparatus that is air saturated, the decrease in oxygen in the tank can be correlated to the oxygen uptake of the beads and the oxygen diffusion coefficient [15]. This method allows rapid assessment of the oxygen diffusion coefficient on short time scales. However, bead formation with certain types of hydrogels can be complex, and the method does not allow monitoring of oxygen tension in selected regions of the hydrogel. Other methods more common in current literature involve the use of fluorescent oxygen probes where the fluorescent intensity changes as a function of oxygen levels. Thotherthod often uses the oxygen probe in the form of a dye or microsensors [13,14]. These methods can provide a moderately accurate way to measure the oxygen diffusion coefficient that can also provide oxygen mapping and local variations. However, this approach typically requires specialized equipment, can be expensive, and may require additional calibrations steps. Other methods involve the use of electron spin probe resonance (ESR) microimaging [88]. Oxygen interacts with the spin probe to change the relaxation time which is detected during ESR oximetry. This method is accurate at determining the oxygen diffusion coefficient and can provide spatial oxygen profiles and can work with living cells without causing viability issues. It is expensive since it requires specialized equipment, custom parts, and reagents. Moreover, it tends to have poor spatial resolution, and calibration can change between spin probe batches [88]. Another method uses micro-computed tomography (μCT) data and numerical models to reconstruct the porous structure through a simulation. The oxygen diffusion

coefficient can then be calculated from the porosity of the structure [89]. The benefits of this method is it can be used on a range of materials, such as scaffolds, various types of tissues, and bioactive glass. It also provides much more information about the structure instead of just the oxygen diffusion coefficient. The cons are that it requires μCT data and access to specialized equipment, and while theoretically it could work on hydrogels it has not been tested to our knowledge.

Table 1 Advantages and drawbacks of current methods to measure oxygen diffusivity in hydrogels and scaffolds

Method	Description	Advantages	Disadvantages
Optical	The use of a dye or microsensor with a fluorophore that quenches in the presence of oxygen. Microsensors or the dye are embedded in the hydrogel	• Accurate • Oxygen mapping and local variations capabilities	• Requires specialized equipment. • Can be expensive (depending on the dye or commercial sensor) • Can require additional calibration steps
Stirred Tank	Deoxygenated hydrogel beads are stirred in a closed tank. The oxygen reuptake is monitored with a probe and correlated to the diffusion.	• Simple and easy to use • Established • Reliable • Fast response	• Not suitable for all formulations of hydrogels • Limited to bead geometry • Requires custom apparatus • Cannot measure local oxygen variations
ESR	Oxygen interacts with a spin probe and changes its T1 and T2 relaxation time depending on concentration. A hydrogel has the biocompatible spin probe embedded and is measured using electron spin probe resonance in	• Can work with living cells • Provides 3D spatial oxygen resolution • Can work in many geometries	• Can work with living cells • Expensive • Requires specialized equipment and custom parts/ reagents • Poor 3D spatial resolution • Calibration changes between spin probe batches

	3D space. This is also known as ESR oximetry		
μCT	Micro CT data is used to reconstruct the scaffold/ tissue structure using computational methods and simulation. The structure and porosity is then used to determine the diffusivity.	• Works with a variety of materials • Provides more information about structure of material (e.g. porosity)	• Requires μCT data and access to specialized equipment. • Has not been tested on hydrogels yet

Many papers discuss the macromolecule diffusion like glucose through hydrogels, and this process is a bit simpler. It generally involves two chambers that are divided by the hydrogel, the concentration difference drives diffusion between both chambers which is recorded over time [90,91].

The oxygen diffusion coefficient can also be determined as a fitting variable in a cellular system using an oxygen scavenger in the media [16]. Effectively, the oxygen scavenger depletes the media of oxygen and the oxygen levels at the base of the hydrogel construct is monitored over time. The advantage of this setup is that it is very accessible since it only requires an oxygen scavenger to control the oxygen levels, and that it is likely much cheaper than buying equipment. A couple of cons of this setup are that the reaction is limited, and if the hydrogel is embedded with cells the diffusion coefficient is measured indirectly as a fitting variable. While this method is a good option for finding a lot of information about a system at a low cost, it could also lead to larger errors in the diffusivity measurement since other variables are affecting the data.

3 Chapter 3: A simple and accessible method to measure oxygen diffusion in cellular encapsulation devices for type 1 diabetes.

3.1 Preface

In this chapter, a manuscript called "An accessible method to measure oxygen diffusion in cellular encapsulation devices for type 1 diabetes." which is to be submitted for publication in Acta Biomaterialia is presented. The author list of this manuscript is as follows: K.S. Champion, L. Gauvin, J. Brossard, R.L. Leask, C.A. Hoesli. The manuscript details a simpler and more accessible way to measure the oxygen diffusion in liquids and hydrogels. The oxygen diffusion coefficient of these gels is then used to predict cellular behaviour in mouse insulinoma cells (MIN6). Together, the oxygen diffusion coefficient and the oxygen consumption rate investigated in our previous work [1], were used in a model to find the Thiele modulus and effectiveness factor.

The method for measuring oxygen diffusivity consists of depleting a gel or liquid of oxygen over a fixed time and monitoring the oxygen depletion in a known position on a 1D line. Using Fick's law, the experimental data is fitted to an oxygen diffusion coefficient. The system boundary conditions were verified using computational fluid dynamics (CFD), and the system was validated by measuring the well-known oxygen diffusion coefficient of water at 37°C. In current literature, the accepted value is approximately 3.1×10^{-5} cm^2s^{-1} ($2.9\text{-}3.3 \times 10^{-5}$ cm^2s^{-1}), while this paper finds the value at 3.2×10^{-5} $cm^2s^{-1} \pm 0.5 \times 10^{-5}$. In performing the same testing on various hydrogels, the findings suggest that an alginate slab that is internally gelled with 5% w/v Manugel GHB is the least diffusive of the tested materials ($D_{O2} = 1.1 \times 10^{-5}$ $cm^2s^{-1} \pm 0.4 \times 10^{-5}$ $cm^{-2}s^{-1}$) and alginate slabs gelled with 2% 10/60 Protanal to be the most diffusive ($D_{O2} = 2.7 \times 10^{-5}$ $cm^2s^{-1} \pm 0.4 \times 10^{-5}$ $cm^{-2}s^{-1}$). The values found in this work are within the range of feasible oxygen

diffusion coefficients for hydrogels as many currently assume alginate to have a diffusion of ~$2.5x10^{-5}$ cm^2s^{-1}.

After measuring the oxygen diffusivity for different hydrogels, MIN6 cells were encapsulated in the different materials to assess their effect on viability. Using modelling parameters like the OCR, Thiele modulus, and effectiveness factor. The results ultimately demonstrated that the trends seen in MIN6 cell viability at different cell fractions was consistent with modelling theory.

3.2 Abstract

Cellular encapsulation in a hydrogel facilitates the 3D immobilized cell culture and the development of cellular therapies for various diseases like diabetes and cancer. However, cellular encapsulation can lead to hypoxia as a result of oxygen mass transport limitations, which is especially true for islet encapsulation in treating diabetes. In turn, hypoxia limits cell survival and function, making the therapy less effective. To improve the design of these therapies, critical oxygen transport parameters like the oxygen diffusion coefficient in hydrogels need to be measured. In this work, a simple system was developed to measure the diffusion coefficient of alginate hydrogels to assess their impact on cell oxygenation. The system was validated by first verifying the surface boundary condition with computational fluid dynamics and the Peclet number to ensure the system is diffusion driven, followed by measuring the diffusion of water (37°C; $3.2x10^{-5} \pm 0.5x10^{-5}$ cm^2s^{-1}). The diffusion coefficient for 3 formulations of alginate hydrogels were measured and compared. The difference in encapsulation materials showed significant differences in MIN6 cell viability at lower cell fractions (1.2 million cells/mL) but not at high cell fractions (10 million cells/mL). This trend in viability with cell fraction is consistent with the theory using the relationship between the Thiele modulus and effectiveness factor. This

work will help design encapsulation devices by benchmarking the oxygen diffusivity of encapsulation materials and suitable cell fractions.

3.3 Introduction

Hydrogel-based cellular encapsulation is an immensely versatile technique that has been widely adopted across diverse fields of study. It has countless applications ranging from 3D cell culture to the development of treatments for a wide range of diseases, including cancer, acute liver failure and diabetes [2–4]. The hydrogel used for encapsulation can serve as a delivery mechanism for stem cells which in turn can deliver therapeutic doses of molecules like insulin in the case of diabetes [2] or anti-tumor agents in the case of cancer treatment [4]. One common thread amongst all these treatments is the use of cells, and the importance of oxygen diffusion in maintaining cell viability. Encapsulating cells can create a diffusion barrier for oxygen which could in turn leads to hypoxia and cell death, rendering the cellular therapy less effective. One good example of a cellular therapy with oxygen diffusion limitations is islet transplantation and islet encapsulation [1,5–7].

Islet transplantation is a cellular therapy that has the potential to allow diabetic patients to become insulin independent [8–10]. Currently this therapy is in phase 3 human clinical trials and the FDA has endorsed a cell transplantation product for brittle type 1 diabetes [10–12]. However, current therapies involve the use of immunosuppression to prevent islet rejection which can cause adverse side effects [13,14]. Islet encapsulation does not require immunosuppressants, since the hydrogel creates a shield that blocks the natural immune function of larger entities like cytotoxic T cells and auto-immune antibodies but allows small nutrients, oxygen, glucose, and insulin to pass [15,16]. While this technique is still experimental, it has demonstrated great potential in practice and has treated diabetes in mice [17]. Alginate hydrogel encapsulation has

also shown to provide long-term immunoprotection in primates, and has progressed to human clinical trials [18,19].

A major concern with all islet transplantation therapies is is limited oxygen diffusion and hypoxia [1,5–7]. Islets natively have a very complex angioarchitecture to ensure all the cells are being adequately oxygenated by blood as a result of their highly aerobic nature [7,20]. After isolation from a donor, this native vasculature is disrupted. The cells at the core of avascular islet clusters rely solely on the external diffusion of oxygen making them much more vulnerable to hypoxia. This issue is exacerbated when encapsulating the cells in a hydrogel due to the addition of another external oxygen diffusion boundary [7]. The type of encapsulation also affects hypoxia, when many islets are encapsulated together in a discrete device (macroencapsulation) there is more local competition for oxygen compared to when the islets are individually encapsulated (microencapsulation) assuming that oxygen concentration is uniform at the boundary of each device. Macroencapsulation has the advantage of being a retrievable medical device with a large variety of geometries (perfusion channels, rods, external diffusion patches, etc.) that can be optimized for better performance and oxygenation [1,15,21].

An *in silico* approach has the potential to significantly reduce cost and time of prototyping during the design phase of various medical devices and is widely applicable. Due to the scarcity and cost of isolated islets, computational models are a very useful tool in early development of macroencapsulation devices. Several models have been developed for islet oxygenation both with and without encapsulation [22–25]. Some of the critical parameters for these types of models include: the cell fraction, the oxygen consumption rate (OCR) of the modelled cell(s), or the oxygen diffusion coefficient of the surrounding medium (ex: cell media, hydrogels, etc.). A current limitation are that modelling parameters are most often assumed due to a lack of

experimental data [26]. Quantifying parameters, such as the oxygen diffusion coefficient, is non-trivial but necessary owning to their significant impact on the simulation and variation even within a class of hydrogels. The aim of this work is to develop a simple method to measure the oxygen diffusion coefficient for encapsulation therapies.

Existing methods for experimentally measuring the oxygen diffusion coefficient of hydrogels require complex apparatus and specialized equipment. One of the easier methods involves measuring the decrease of oxygen in a stirred tank apparatus after adding previously deoxygenated calcium alginate gel beads [27]. The pros of this method is that its simple and easy to use, and can reliably measure the oxygen diffusion coefficient with a fast response. The cons are that it may not be suitable for all types of hydrogels depending on how they are formulated and can only work with beads. Moreover, it cannot record localized oxygen variations in a hydrogel. More modern methods involve the use of probes like spin probes for electron spin resonance (ESR) microimaging [28] or optical oxygen dyes and microsensors [29–31]. The pros of these methods are that they provide an accurate way to measure the oxygen diffusion coefficient. The cons are that they both require specialized equipment which can be expensive and may require additional calibrations steps. Another method to measure oxygen diffusivity uses numerical methods to estimate the oxygen diffusion coefficient used micro-computed tomography (μCT) data [32]. The pros of this method is it can be used on a range of materials, such as scaffolds, various types of tissues, and bioactive glass. It also provides much more information about the structure instead of just the oxygen diffusion coefficient. The cons are that it requires μCT data and access to specialized equipment, and while theoretically it could work on hydrogels it has not been tested to our knowledge. Although these methods are effective in measuring oxygen diffusivity, they are not easily accessible, hard to implement in multiple

materials or require limiting assumptions. This paper will focus on developing a simple and accessible method to measure the oxygen diffusion coefficient in liquids and hydrogels which could be useful for numerical model refinement, medical device design optimization, etc.

3.4 Materials and Methods

3.4.1 System to measure oxygen diffusion coefficient

The setup to measure oxygen diffusion is shown in Fig. 3-1A flow cap shown is attached to a glass Petri dish (Ø 50 mm; Pyrex) to control the oxygen tension at the surface and have negligible oxygen diffusion at the bottom (glass). An oxygen sensing needle probe (OX500PT; Pyroscience) is fixed in place at the center of the system using a universal stand and jack, which measures the local oxygen level at the height of the probe (Fig. 3-1C). To improve the measurement accuracy, the Petri dish setup is placed in a temperature-controlled environment (Fig. 3-1A). The gas entering the Petri dish is a mixture of : nitrogen (N_2), air (79% N_2, 21% Oxygen (O_2)) , and carbon dioxide (CO_2). CO_2 was provided through volumetric control of a flowmeter (Cole-Parmer; 03227-04), while larger capacity flowmeters (Cole-Parmer; 03227-12) were used to regulate the amounts of both N_2 and air. The gases are mixed and sent into a heated humidifier to control the gas temperature and humidity to finally be delivered into the Petri dish.

The oxygen probe is first calibrated using a 2-point calibration in the Pyroscience O2Logger software, the two points are: (i) 0% O_2 using water with an oxygen scavenger commercially available known as OXCAL (Pyroscience) and (ii) air-saturated water at a set temperature in the software corresponding to the temperature measured with an alcohol thermometer. The temperature-controlled box was set to 37°C and all liquid or hydrogel samples were equilibrated in an incubator before testing (37°C; 5% CO_2) . The gas line was purged with 100% N_2 at 300

mL/min for 10 min, then the flowrate was reduced to 130 mL/min. The OX500PT probe needle was gently placed into the Petri dish sensing port.

A syringe with a 15-gauge needle was used to inject the sample (liquid or hydrogel) into the Petri dish around the probe, while taking note of the exact volume added. Initial gas bubbles formed at tip were removed by flicking the probe. The oxygen measurements were logged in the software with a sample rate of 9s, continuous data logging, with no data smoothing . After waiting 5-10 min for system stabilization (vibration, temperature, etc.) the N_2 purged gas line set to 130 mL/min was attached to the Petri dish, while taking note of the time on the logging software. Over time, the oxygen present should slowly decrease and captured in the software. Note that if the experiment was performed with a hydrogel, an experimental check using water was reperformed and the beginning or in between experiments to confirm that the system is still measuring diffusivity correctly.

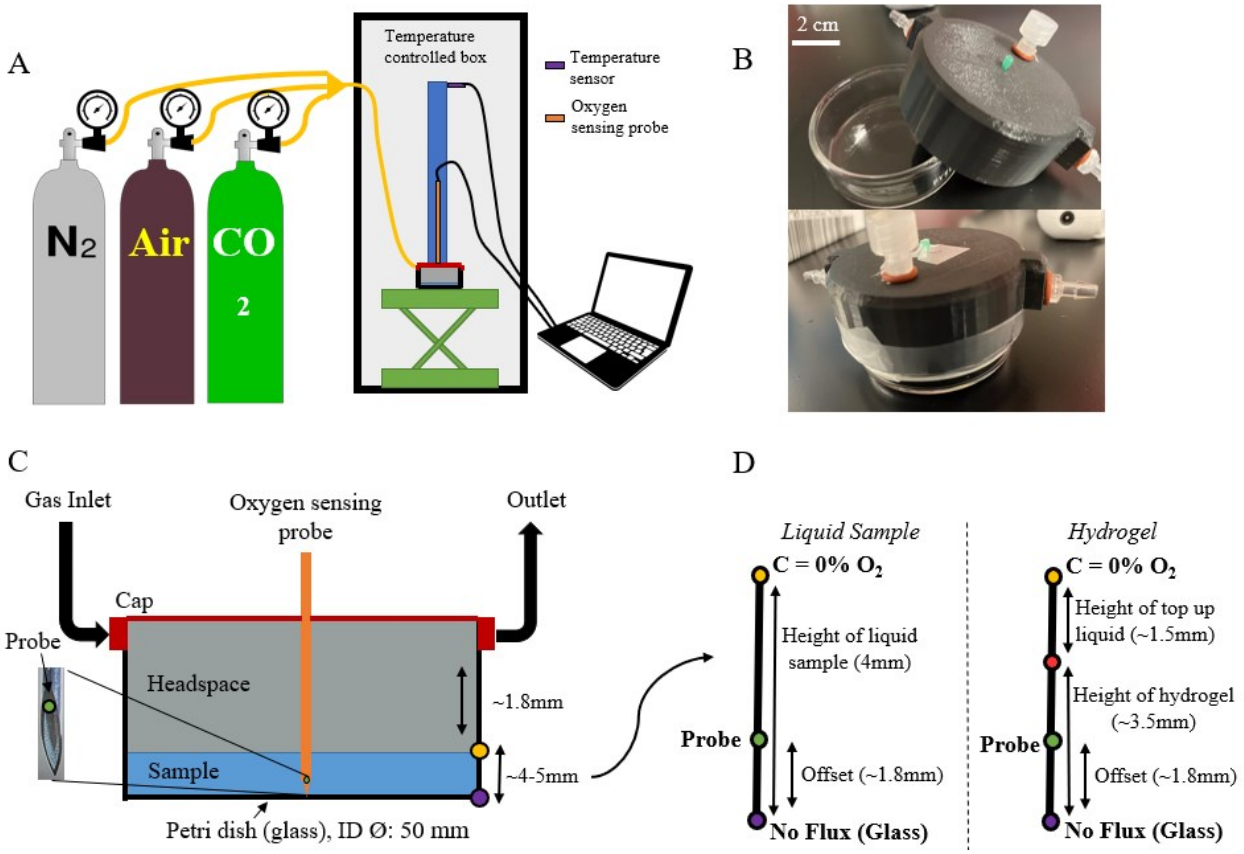

Fig. 3-1 System setup and modelling approach

(A) Exterior system setup. Three blended gases (CO_2, N_2, Air) are fed into the Petri dish and oxygen is monitored. Setup is fully enclosed in a temperature-controlled environment. (B) Close up images of Petri dish system when open and sealed closed with parafilm. (C) Technical diagram of cross-sectional view in Petri dish setup with relevant measurements for modelling. (D) Close up on the sample in the Petri dish. 1D diffusion model for liquid samples and hydrogels including boundary conditions and modelling relevant measurements. Hydrogel samples include a small amount of top up media to prevent the gel from drying out. The liquid/hydrogel interface is shown in red.

3.4.2 Computational modelling and governing equations

All modelling was performed in COMSOL Multiphysics 5.6. The modelling was performed in two steps: (1) the boundary condition verification which makes use of the 2D time independent laminar flow module, and (2) the diffusion coefficient numerical model which makes use of the 1D time dependent transport of dilute species module.

3.4.3 Boundary condition verification using computational fluid dynamics

The 2D laminar flow module was used to model the gas flow profile in the headspace between the hydrogel/fluid and the cover of the glass Petri dish. In turn, this model can estimate the water surface velocity and provide an estimate for the Peclet number to determine if the system is diffusion driven. A 2D geometry was used for improved mesh resolution and corresponds to the center plane of the Petri dish where the oxygen probe is located. The simulation assumes no backflow or pressure loss, no slip condition at the Petri dish rigid walls, steady-state, Newtonian fluid, incompressible fluid (air and liquid region), and fully developed laminar flow at the inlet. The boundary layer at the surface of the liquid was taken as an air-liquid interface. The boundary conditions are: (1) normalized laminar flow at the inlet (flowrate per known inlet length scale). (2) zero pressure at outlet (results in gauge pressure profile), and the model is at steady state (time independent). Note that the length scale used to normalize the flowrate was determined by the inner diameter in the inlet tubing, which is 4mm. An "extremely fine" mesh was used for all calculations (45830 elements; size of $5x10^{-4}$ to 0.168). The governing equations for solving the velocity and pressure profile is the 2D cartesian time independent Navier-Stokes equation, and the conservation of mass (continuity equation). The shear stress profile was found by calculating the product of the shear rate and viscosity (both calculated by COMSOL natively).

The Peclet number (Pe) is the ratio of advective mass transport to diffusive mass transport. It was calculated using the perpendicular surface velocity (u) found from the model at the air-liquid interface boundary layer, the characteristic length (L) which was taken as the height of liquid sample, and the diffusion coefficient (D).

$$Pe = \frac{advective\ transport}{diffusive\ transport} = \frac{uL}{D}$$

If Pe<1, in general this would suggest that the system is diffusion driven and that recorded data is predominantly a result of diffusion.

3.4.4 1D time dependent mass transfer model

The 1D transport of dilute species module in COMSOL 5.6 was used to model the oxygen depletion across the center axis of the Petri dish where the oxygen probe is located. The boundary conditions for this line are presented in Fig. 3-1D. An extremely fine mesh (45830 elements; size of $5x10^{-4}$ to 0.168) was used to solve all numerical models, and all reaction terms were ignored since these experiments were acellular. The governing equation for this modelling is Fick's law:

$$D\frac{\partial^2 c_{O_2}}{\partial z^2} = \frac{\partial c_{O_2}}{\partial t}$$

Where z is the length along the center axis where the probe is located.

For a liquid, the top of the line in contact with the gas-controlled boundary condition is assumed to have an oxygen concentration of 0 (C= 0 mol/m^3) or to follow the transfer function experimentally determined in Fig. 3-2E. The opposite end in contact with glass is assumed to have a no flux boundary condition. This assumption is valid since glass has an oxygen diffusion coefficient that is orders of magnitude lower than water and hydrogels. For hydrogel modelling,

an additional interface exists between the top up media and hydrogel as shown in Fig. 3-1D. Media is assumed to have the same diffusivity as water at 37°C. The probe offset location is determined experimentally and corresponds to where the model is compared to experimental data. The offset distance from the tip of the needle to the beginning of the probe (sheathed within the needle) was measured using a caliper and microscope.

3.4.5 Thiele Modulus and Effectiveness Factor Calculations

The Thiele modulus (φ) describes the relationship between the reaction rate and the diffusion rate in mass transfer for porous materials like hydrogels.

The oxygen consumption in islets was assumed as a 0^{th} order reaction where the cells fixed oxygen consumption rate. 0^{th} order kinetics can be assumed if the ratio between the Michaelis-Menten coefficient and surface concentration approaches 0 ($\frac{K_m}{C_s} \cong 0$) [33]. Islets have a Michaelis-Menten coefficient of ~0.44 mmHg for oxygen consumption [22,34] which is much less than the surface oxygen tension of ~80-140mmHg (~10-18.6% O_2). As a result, assuming the reaction is 0^{th} order is a valid assumption in this work since the Michaelis-Menten coefficient is much less than the surface oxygen concentration ($K_m << C_s$).

The Thiele modulus for a simple 0^{th} order system was derived from [35]. It was calculated with a constant reaction rate (k_v) equal to the cellular oxygen consumption rate (OCR) normalized by cell fraction (X), and surface oxygen concentration (C_s) and is presented as the following:

$$\varphi = \frac{reaction\ rate}{diffusion\ rate} = \frac{V}{SA}\sqrt{\frac{k_v}{2D_{eff}C_s}} = L\sqrt{\frac{X(OCR)}{2D_{eff}C_s}}$$

The effectiveness factor (η) is a non-dimensional number between 0 and 1 that generally helps understand how much a system is limited by mass transfer, in this case it would describe how well the cells are being oxygenated. If oxygen is in abundance and can travel freely into the cells, the effectiveness would be 1. If oxygen cannot diffuse fast enough into the cells because of mass transfer limitations of the material, this would result in a low effectiveness factor (close to 0).

The effectiveness factor was calculated from literature for a slab geometry with a 0^{th} order reaction [36]. Note that for this derivation, φ_{crit} is taken as $\sqrt{2}$ [36].

$$\eta = \begin{cases} 1 & ; \phi \leq \phi_{crit} \\ 1 - \dfrac{\sqrt{\phi + 2}}{\phi} & ; \phi > \phi_{crit} \end{cases}$$

3.4.6 Adherent cell culture

Mouse insulinoma 6 (MIN6) cells in complete medium were seeded in tissue culture treated polystyrene flasks until 80-90% confluency. The cell medium consisted of Dulbecco's Modified Eagle medium (DMEM; Gibco #10313-021, Thermo Fisher Scientific) supplemented with 10% fetal bovine serum (FBS; HyClone #SH3039602, Fisher Scientific), 1% L-glutamine (Gibco #25030-081, Thermo Fisher Scientific), 1% penicillin/streptomycin (Gibco #15140-122, Thermo Fisher Scientific), and 0.1% 2-mercaptoethanol (Fisher Chemical #O3446I, Fisher Scientific). Changes were performed every 48-72 h. An incubator at 37°C and 5% CO_2 was used to culture the cells. Passaging was performed using 1X TrypLE Express Enzyme (Gibco #12605-028, Thermo Fisher Scientific). All cells used had a passage number between 28 and 40.

3.4.7 Production of alginate slabs

Alginate slabs were produced using internal gelation. The two types of alginates used in this work were Manugel GHB (IFF Nutrition & Biosciences (formerly FMC Biopolymer) through DuPont), Protanal 10/60 LF (IFF Nutrition & Biosciences (formerly FMC Biopolymer) through DuPont). A stock solution of either 2.5% w/v Manugel GHB, 2.5% w/v Protanal, or 6.25% w/v Manugel GHB was prepared in pH 7.4 HEPES-buffered saline (170mM NaCl; 10mM HEPES). The alginate stock solution was autoclaved at 121°C for 30 min, 100mL of the stock solution was autoclaved each time. A second stock solution of 0.5 M calcium carbonate ($CaCO_3$; Avantor #1301-01, VWR) was also prepared in pH 7.4 HEPES-buffered saline and sonicated for 15 min to break up any calcium carbonate that has aggregated. This solution was autoclaved at 121°C for 30 min. Glucono-δ-lactone (GDL; Sigma-Aldrich #G4750, MilliporeSigma) was dissolved in HEPES-buffered saline and sterilized with a 0.2-µm nylon syringe filter (Fisherbrand™ #09-719C, Fisher Scientific) immediately before use.

To prepare a slab with a height of at least 4 mm with a 50 mm diameter, at least 5.6 mL of alginate solution is necessary. For all experiments, 10 mL of alginate hydrogel mixture was made. 8 mL of 2.5 % alginate or 6.25 % alginate with 0.6 mL of the 0.5 M $CaCO_3$ solution were mixed in a 10mL syringe with the plunger removed and the bottom capped. A 1 mL solution of cell culture media containing trypsinised MIN6 cells that will result in the desired final cell concentration was then added to the syringe. Finally, 0.6 mL of the GDL solution was added to the syringe. The resulting solution is ~2% or ~5 % w/v alginate stock, 30 mM $CaCO_3$, and 60 mM GDL. The syringe plunger was then reintroduced, while preventing any alginate solution from leaking out. The solution, 7.9mL, was injected and evenly spread into glass Petri dish (Ø 50 mm), note that 7.9mL

corresponds to a 50 mm cylinder with a 4 mm height (characteristic length used for Pe and modelling).

The slabs were left to gel for between 30-40 min (until visually solid) and topped up with 4mL of cell culture media to prevent the slab from drying out. The Petri dish is then sealed with a piece of parafilm that was previously soaked in ethanol. The slabs were placed in an incubator at 37°C and 5% CO_2 for 16-24h.

3.4.8 Live/dead staining & image acquisition

After the slabs underwent 16-24h of incubation, a very thin vertical slice of the center of the slab was cut using a razor blade and stained using a live/dead solution with final concentrations consisting of 18.9 µg/mL propidium iodide (Fisher Scientific; P1304MP) and 1.1 µg/mL Calcein AM (Fisher Scientific; C1430) both in pH 7.4 HEPES-buffered saline at room temperature. Images were acquired using an IX81 Olympus Microscope at 10X magnification on the full chip setting using a FITC filter cube (Ex: 482/35 | Em: 536/40) and a Texas Red filter cube (Ex: 525/40 | Em: 585/40). The exposure time used for all imaging was 100ms.

3.4.9 Image analysis for live/dead staining

Images were stitched in a grid-wise format using a stage file generated in MATLAB^{tm} [37], a step size of 850µm in the X and Y direction. Live/dead fluorescence analysis and live MIN6 cells depth analysis was performed in FIJI (ImageJ). Acquired images were cropped from 2048x2048 pixels to 1550x1550 pixels and stitched column-by-column, up-and-right, with an overlap of 18% using the built-in stitching function [38]. FITC and Texas Red images were merged where FITC was chosen to be green and Texas Red which was red. Live MIN6 cells depth analysis was performed by setting a calibrated scale of 1300 pixels:850 µm and by visually measuring the live height (the

green portion) and total slab height at the top, middle, and bottom of the slab using the line tool in ImageJ.

3.4.10 Statistics and Plotting

All averages and standard deviations were computed using Microsoft Excel. The data was plotted in either Excel or in GraphPad Prism. All data was checked for normality in GraphPad using the Shapiro-Wilk test ($p \geq 0.05$). To evaluate differences between experimental groups, a one-way ANOVA was performed, followed by the Tukey test to compare groups. All tests used a 95% confidence interval ($\alpha = 0.05$).

3.5 Results

An accessible way to measure the oxygen diffusion was developed in this work. Using an oxygen probe and conventional laboratory equipment, the oxygen diffusivity of various hydrogel formulations was measured. One of the main assumptions in this measurement method is that the probe is measuring a system that is diffusion dominant with negligible advective effects. To verify negligible advection, a computational fluid dynamics (CFD) model of the headspace was developed to determine the Peclet number (ratio of diffusion to advection).

3.5.1 CFD model of headspace and boundary condition justification

To correctly measure the oxygen diffusion coefficient, the experimental system must be diffusion driven, and the mass transfer model must have proper boundary conditions which reflect the experimental setup. A model for the cross-section of the Petri dish with the headspace from the cap included was modelled as shown in Fig. 3-2A. This model simulates the gas flow above the liquid or hydrogel and is used to determine if the system is diffusion driven. Fig. 3-2B and Fig. 3-2D show the velocity profile and shear stress profile for a sample that has a

characteristic length of 4mm (a sample of 7.9 mL). The main assumption with this modelling is that the flow profile experienced by the oxygen probe is the same as the flow profile across the center plane of the Petri dish where the probe is located, the modelling limitations include the edge effects resulting from the curvature of the Petri dish, and any vorticity or secondary flow patterns occurring in 3D space.

The advantage in making this assumption is the 2D model can have a much finer mesh and lower relative tolerance, leading to improved numerical accuracy of the surface velocity of the liquid/hydrogel sample and Peclet number approximation. Moreover, this assumption is conservative as the velocity at the center of 2D plane would be higher than in a 3D Petri dish since there would be more area for the inlet to expand.

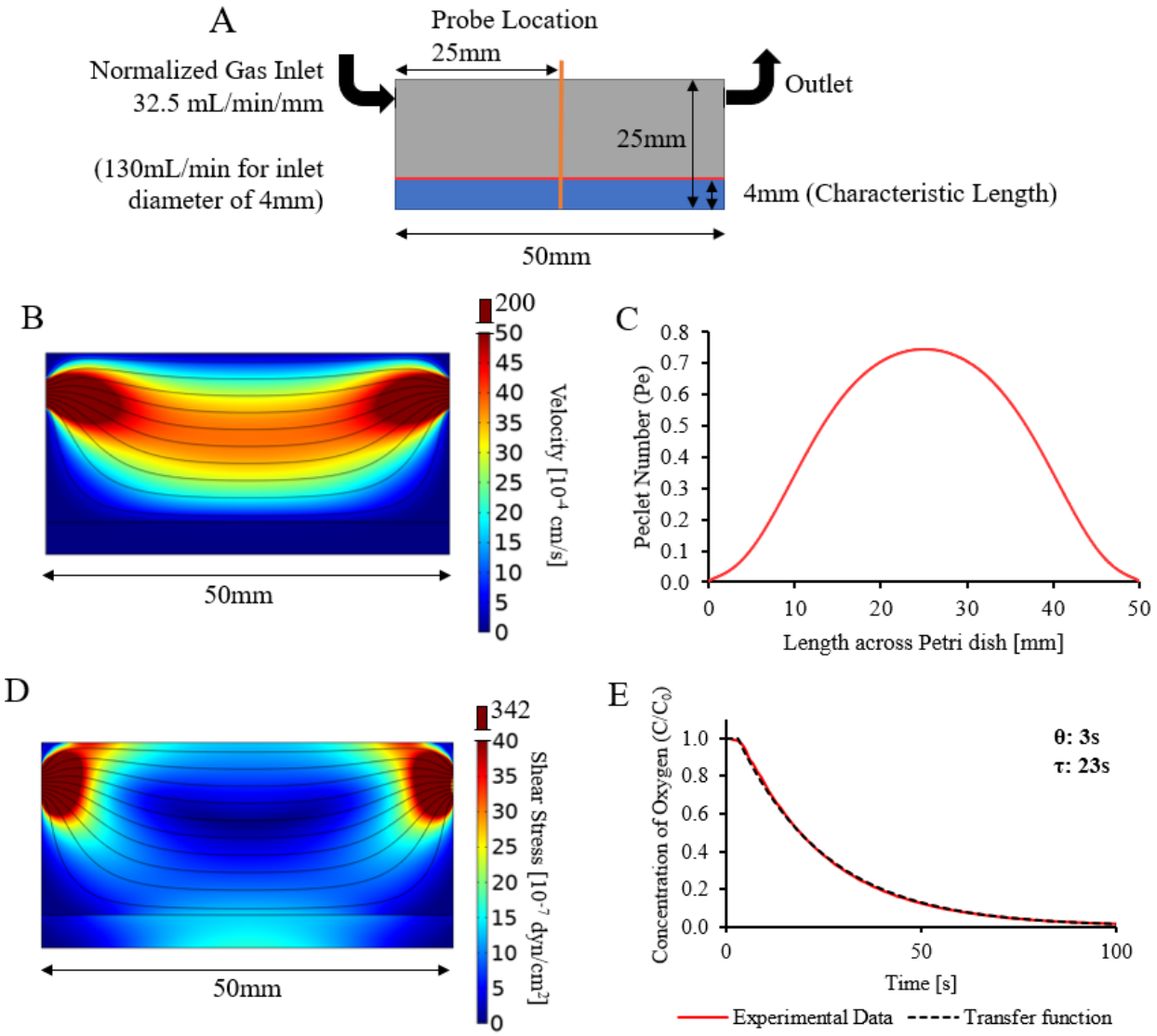

Fig. 3-2 Mass transfer modelling boundary condition justification and assessing advective effects of headspace flow profile.

(A) 2D geometry simulating the flow profile along the central cross-section of closed Petri dish system with a 50 mm ID Ø, and a gas inlet/outlet port of 4mm ID Ø (D_h = 4mm). Includes a sample with a characteristic length of 4mm. The red line illustrates the gas-liquid across the center of the Petri dish. (B) The velocity magnitude profile (colour map) and streamlines (black) of Petri dish cross section [cm/s]. Colour scale is zoomed in to highlight profile at lower velocities (Shown range: 0 to 50 cm/s, actual range: 0 to 200 cm/s). (C) The Peclet number (Pe) along the gas-liquid interface (shown in red).

Calculated using the perpendicular velocity component (u), the characteristic length (L = 4mm), Pe = uL/D_{water} where D_{water} = ~3.1x10^{-5} cm^2/s. Average Pe is 0.48 < 1, max Pe is 0.75

< 1. (D) The shear stress profile (colour map) and streamlines (black) of Petri dish cross section [dyn/cm^2]. Colour scale is zoomed in to highlight profile at lower velocities (Shown range: 0 to 40 dyn/cm^2, actual range: 0 to 342 dyn/cm^2). (E) Experimental transfer function for non-dimensional oxygen concentration (C/C_0) the gas-liquid interface to reach 0% O_2 from 21% (atmosphere). This transfer function is first order with a time delay (θ) of 3 seconds and a time constant (τ) of 23 seconds.

With the computed model, the perpendicular velocity at the air-liquid interface shown in Fig. 3-2A can be used to calculate the Pe number across the Petri dish (shown in Fig. 3-2C). The average Pe was 0.48 and the maximum was 0.75, both of which are less than 1 indicating the system is diffusion dominated. To verify the assumption in the mass transfer model that the surface of the hydrogel or water at 0% O_2, the boundary should decrease rapidly to 0% upon a step change. In Fig. 3-2E, the experimental transfer function for the system is presented demonstrating that the boundary goes from 21% to 0% in roughly 100s. Since experiments occur on the timescale of 1-10h, this would suggest that the 100s transitory period from 21% to 0% is negligible.

3.5.2 System validation with water (37°C)

To validate the system, the diffusion coefficient of water at 37 °C was measured and compared to the well-known literature values mostly ranging from 2.9-3.3x10^{-5} cm^{2}s^{-1} [26,39–42]. For this work, the diffusion coefficient is taken as ~3.1x10^{-5} cm^{2}s^{-1}. If the system can accurately measure a standard that is well reproduced in literature, this would increase the confidence in the measurements the hydrogels.

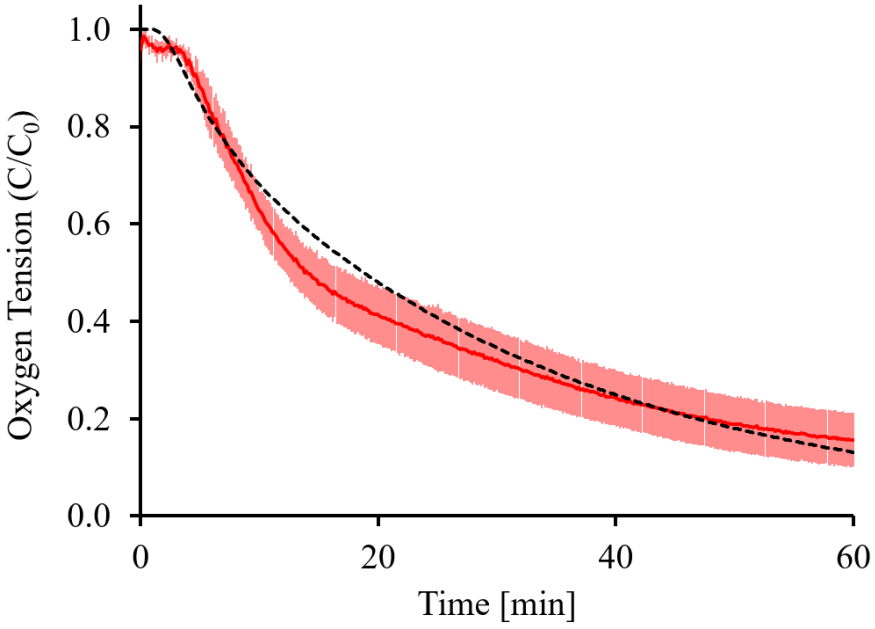

Fig. 3-3 System validation using water at 37°C.

Experimental non-dimensional concentration data (red) of oxygen depletion in air-saturated water (n=7). Numerical model with diffusion coefficient of water at 37°C (D= ~3.1x10-5 cm^2s^{-1}).

The results in Fig. 3-3 indicate that the experimental data is in very good agreement with the numerical model using the literature diffusion coefficient of ~$3.1x10^{-5}$ cm^2s^{-1}, indicating that the system can accurately measure the diffusion coefficient.

3.5.3 Alginate oxygen diffusion coefficient measurements (37°C)

The system was then used to measure the experimental oxygen diffusion coefficients of different formulations of alginate. These formulations include: (1) 2 % w/v Manugel GHB in HEPES, (2) 5 % w/v Manugel GHB in HEPES, (3) 2 % w/v Protanal in HEPES.

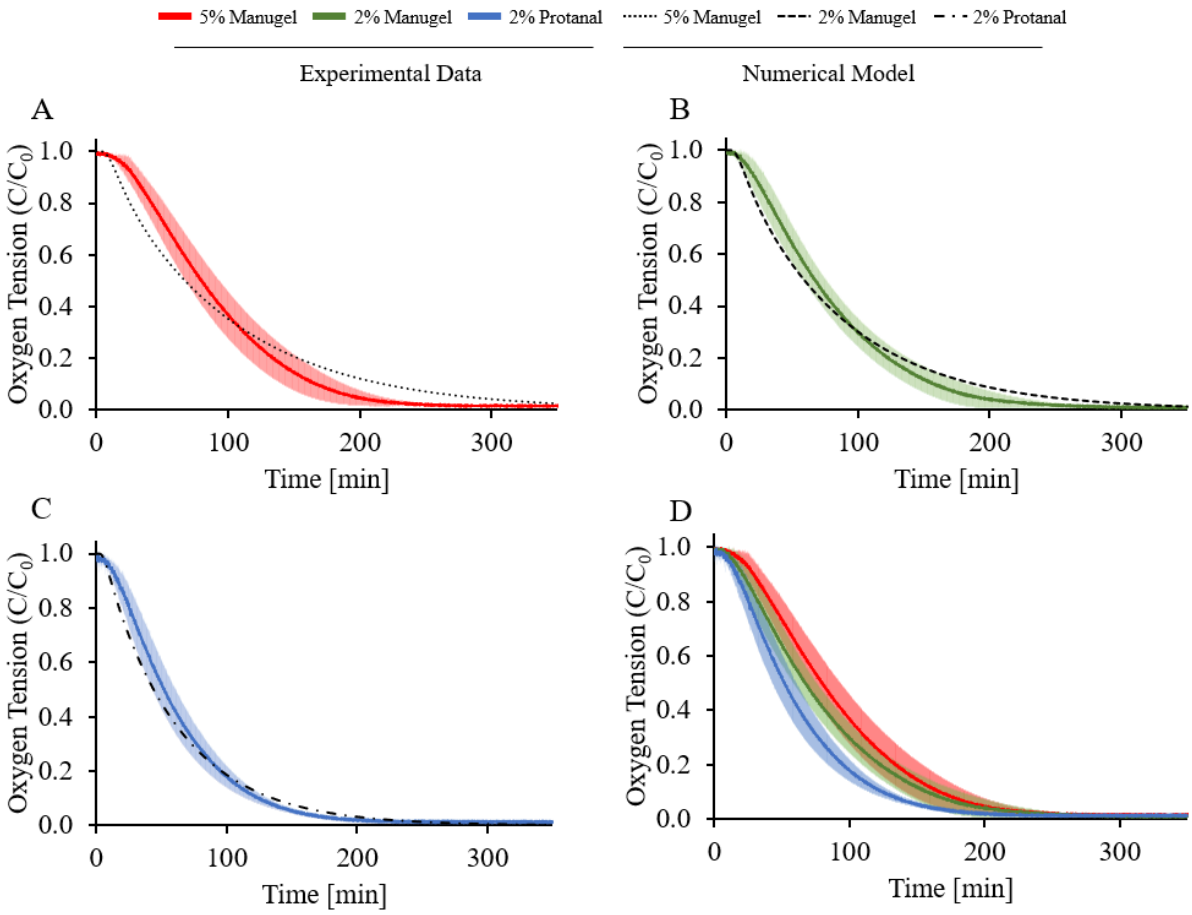

Fig. 3-4 Diffusion coefficient of various alginate compositions at 37°C.

(A) Experimental non-dimensional concentration data (red) of oxygen depletion in 5% w/v Manugel alginate in HEPES buffer (n=3) with numerical model corresponding to D= 1.1x10^{-5} cm^{2}s^{-1}. (B) Experimental non-dimensional concentration data (green) of oxygen depletion in 2% w/v Manugel alginate in HEPES buffer (n=3) with numerical model corresponding to D= 1.5x10^{-5} cm^{2}s^{-1}. (C) Experimental non-dimensional concentration data (blue) of oxygen depletion in 2% w/v Protanal alginate in HEPES buffer (n=3) with numerical model corresponding to D= 2.7x10^{-5} cm^{2}s^{-1}. (D) Overlay of experimental data of all alginate formulations tested.

Oxygen diffusion coefficients from a geometrically correct numerical model were fitted to experimental data by minimizing the mean absolute percent error (MAPE). The average diffusion coefficients for each experiment all illustrated below.

Error amongst the curves follow a pattern shown in Fig. 3-4A, Fig. 3-4B , Fig. 3-4C where the experimental line overshoots the numerical model and rapidly descends afterwards, this is characteristic of a Pe number that is above 1 [43,44], nevertheless the system can still measure the diffusion coefficient with reasonable accuracy (<10-15% relative error between theoretical curves and data). The raw experimental data between alginates is compared in Fig. 3-4D, which would suggest that 2% protanal (blue) is the most diffusive having the fastest rate of deoxygenation compared to 5% Manugel (red) which was the slowest and therefore has the smallest diffusion coefficient. This observation is also supported by the error trends noticed between the models in panels A to C, a material with a lower diffusion coefficient will have more error as the Pe number will be higher. The individual runs were analyzed using a numerical model with a varying diffusion coefficient, whichever value minimized the relative percent error the most was assigned for that run. These results are compared in Fig. 3-5.

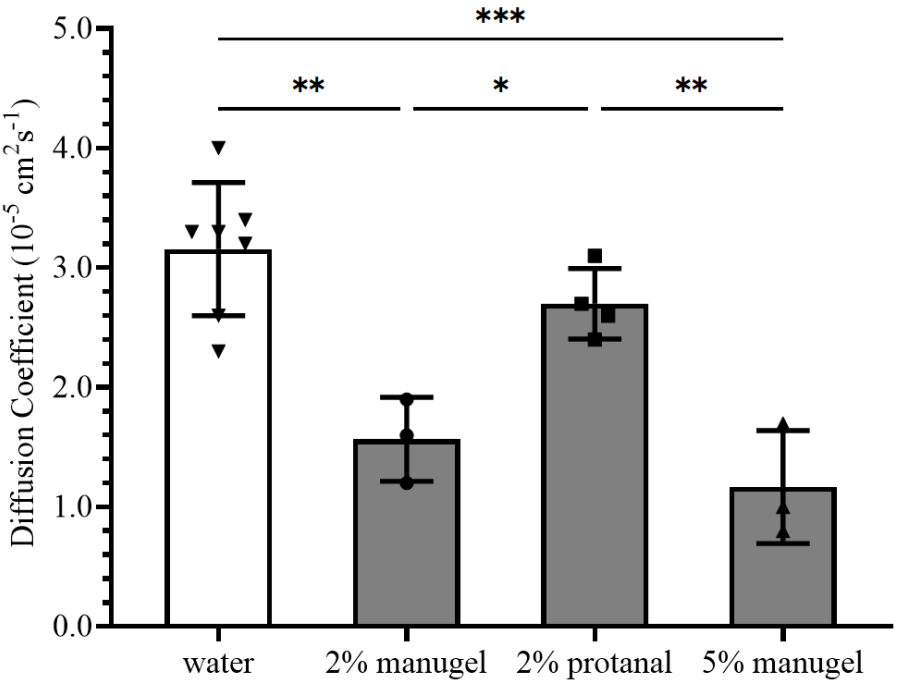

Fig. 3-5 Comparative analysis of diffusion coefficient of various alginate compositions at 37°C.

*Each bar is calculated by taking an average of the diffusion coefficient for each individual run which minimizes the mean average percent error (MAPE). The sample size for hydrogel samples is n=3 for 2% Manugel and 5% Manugel, n=4 for 2% Protanal, and n=7 for water. Significance was assigned as followed: * p≤0.05, ** p≤0.01, *** p≤0.001.*

As expected, the lowest diffusion coefficient of the series was 5% Manugel and the largest (of the hydrogels) was 2% Protanal which is consistent with Fig. 3-4D. Interestingly, there was no significant difference between water and 2% protanal, and no significant difference between 2% Manugel and 5% Manugel. These results illustrate the importance of measuring this parameter as it is variable between alginate compositions.

3.5.4 24h MIN6 cell viability and theoretical cell fractions based on Thiele modulus

Using the equation for the Thiele modulus and effectiveness factor, a theoretical estimation of the maximum cell fraction was determined for different hydrogels and cell types (MIN6 cells vs. islets). An effectiveness factor of 0.9 was chosen as the maximum allowable cell fraction since it theoretically corresponds to a fairly good level of oxygenation where the system is not limited by oxygen diffusion.

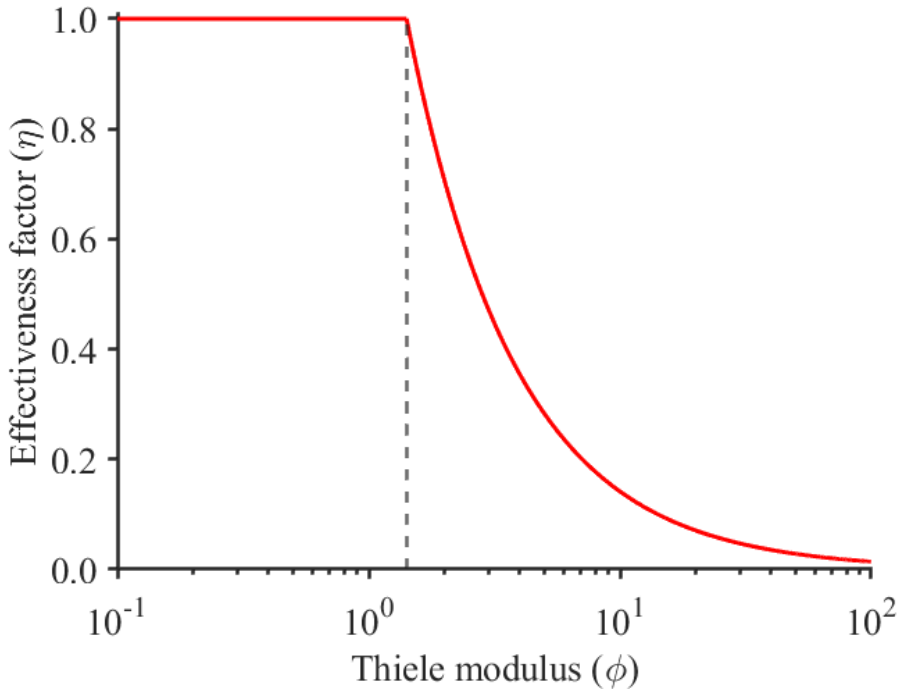

Fig. 3-6 Effectiveness factor for 0th order reaction

The effectiveness factor vs. Thiele modulus plot for a 0^{th} order reaction such as the oxygen consumption of cells when $C_s >> K_m$. Note that the dashed line corresponds to the critical Thiele modulus (φ_{crit}) where the effectiveness begins decreasing from 1.

Since the experiment was done in a simple 1D slab geometry, the effective length (L) is the height of the gel (3.5mm as per Fig. 3-1D). The diffusion (D_{eff}) was taken as a weighted average

using the cell fraction between the diffusion coefficient of tissue ($1.24x10^{-5}$ cm^2s^{-1} [23,39]) and the diffusion coefficient of the material as per Fig. 3-5. The OCR used for MIN6 cells is 0.129 $molm^{-3}s^{-1}$ [1] and 0.034 $molm^{-3}s^{-1}$ [1,22,23,25], note that the MIN6 cells used are from the same cell stock used in [1]. The oxygen surface tension will not always be exactly 18.6% O_2 since there is still a layer of top up media approximately 1.5mm high that oxygen must diffuse through before reaching the top of the slab (as per Fig. 3-1D). To determine the surface oxygen levels of the slab, a separate numerical model was made to develop a relationship between the surface oxygen tension (C_s) and the cell fraction (X) for a given OCR (MIN6 cells or islets) and alginate diffusion coefficient. Finally, a theoretical cell concentration (X) was iterated to yield an effectiveness factor of 0.9, this gives us a rough approximation of the maximum cellular density for a given geometry and encapsulation material.

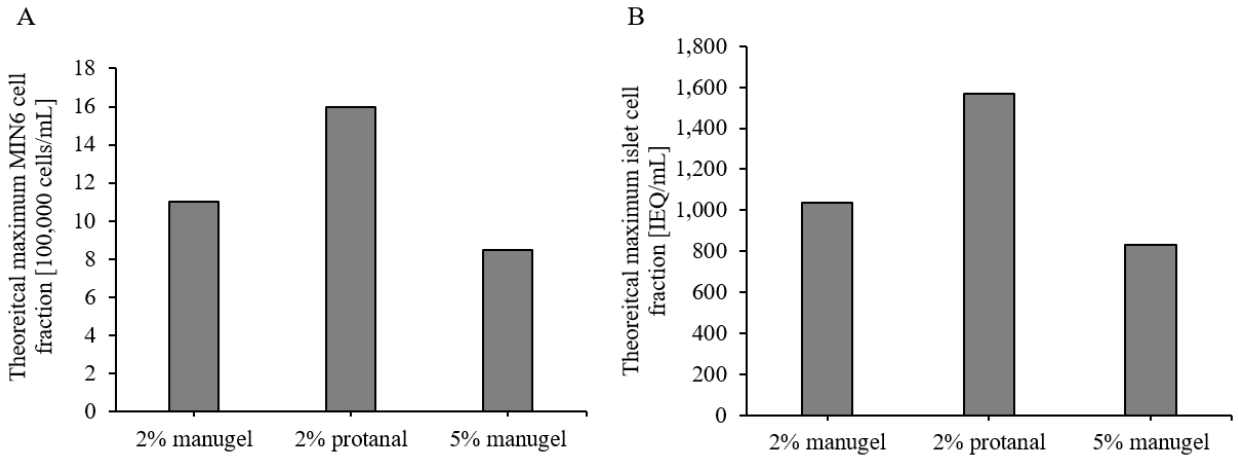

Fig. 3-7 Effect of diffusion coefficient on theoretical maximum cell fraction of MIN6 cells and islets to achieve an effectiveness of 0.9 ($\eta = 0.9$).

(A) Theoretical MIN6 cell fraction needed to obtain an effectiveness factor of 0.9 ($\eta = 0.9$) assuming a constant 0^{th} order cell oxygen consumption rate of 0.129 $molm^{-3}s^{-1}$ (B) Theoretical

islet fraction needed to obtain an effectiveness factor of 0.9 (η = 0.9) assuming a constant 0th order cell oxygen consumption rate of 0.034 molm^{-3}s^{-1}. Islets are assumed to have a 150µm diameter and to be homogeneously distributed.

To determine the relationship between diffusion and cell behaviour, the viability of MIN6 cells in a 1D diffusion slab geometry was evaluated. The experimental viability of MIN6 cells at two different cell fractions is presented in Fig. 3-8.

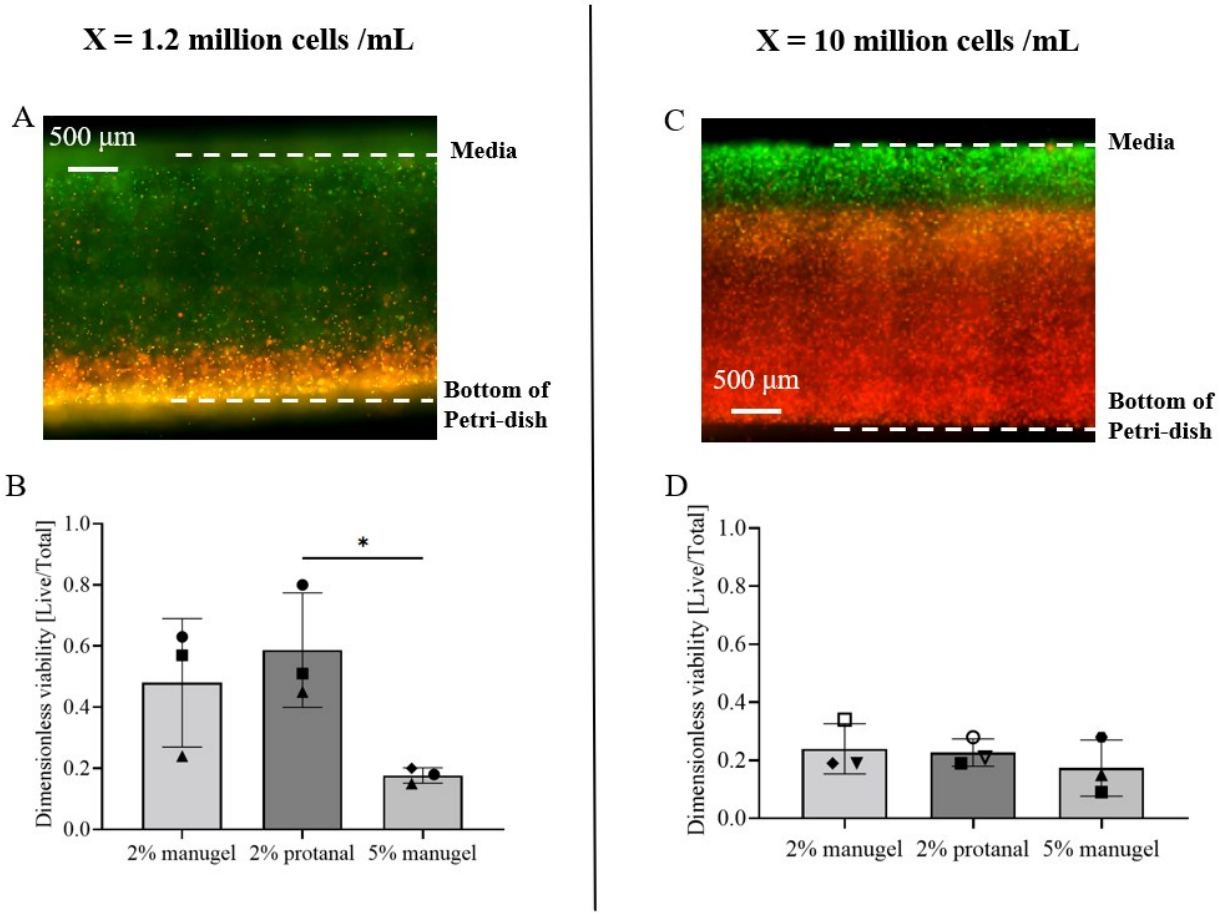

Fig. 3-8 Live/dead analysis of MIN6 cells at 1.2 million cells per mL and 10 million cells/mL

Example image of 2% protanal live/dead cross-section at 1.2 million MIN6 cells/mL. Green indicates live cells (FITC; Ex: 482/35 | Em: 536/40), red indicates dead cells (Texas Red; Ex:

*525/40 | Em: 585/40) after 16-24h of incubation. (B) Dimensionless viability of MIN6 cells at a concentration of 1.2 million cells/mL. Corresponds to the length of the green portion of the slab (live cells) over the total portion. * p≤0.05. (C) Example image of 2% protanal live/dead cross-section at 10 million MIN6 cells/mL. (D) Dimensionless viability of MIN6 cells at a concentration of 10 million cells/mL.*

The dimensionless viability is the ratio of depth of living cells over the entire depth of the slab. The depth of living cells is determined by measuring the length from the top of the slab to where the living (green) cells abruptly changes to dead (red) cells as shown in Fig. 3-8A and Fig. 3-8C. The difference between hydrogels at high cell fractions is less noticeable (Fig. 3-8D) compared to at a lower cell fraction (Fig. 3-8B) where a significant difference was noticed among groups ($p<0.05$). As predicted by the trends in the effectiveness factor, changes in viability would become less noticeable at a higher Thiele modulus and therefore cell fraction by extension. This is due to the non-linearity illustrated in Fig. 3-6.

3.6 Discussion

In this work, we developed a simple and accurate method to measure the oxygen diffusion coefficient of alginate hydrogels, a common hydrogel in encapsulation devices. Then the results were used to predict MIN6 cellular viability. Computational modelling supported the assumption of a diffusion driven apparatus (Pe<1), with a low simulated gas phase velocity above the water and calculated a maximum Peclet number (Pe) of 0.75 (see Fig. 3-2C). Moreover, upon attaching the nitrogen to the system, experimental data showed the concentration of oxygen at the surface of the water declined from 21% to ~0% O_2 completely after about 100s (see Fig. 3-2E), supporting the diffusion driven assumption.

To assess if the system is accurate, the oxygen diffusion coefficient of reverse osmosis water was measured at 37 °C which has a well-known literature value of $\sim 3.1 \times 10^{-5}$ $cm^2 s^{-1}$. The system discussed in this work measured the diffusion coefficient to be 3.2×10^{-5} $cm^2 s^{-1} \pm 0.5 \times 10^{-5}$ $cm^2 s^{-1}$ suggesting that the system can measure the oxygen diffusion coefficient with good accuracy (see Fig. 3-3 & Fig. 3-5). To our knowledge, the oxygen diffusion coefficient of water has been documented to be as low as 2.6×10^{-5} $cm^2 s^{-1}$ [42] and as high as 3.83×10^{-5} $cm^2 s^{-1}$ [45] in literature, indicating that the value we observed in the system is acceptable. The small temperature variations could be part of the cause for small discrepancies in the diffusion coefficient. The error between the model and experimental data in Fig. 3-4 (most dominantly in Fig. 3-4A) appears to be characteristic of a larger Peclet number [44] and is likely an effect of neglecting advection in less diffusive materials. 2% Protanal (Fig. 3-4C) has a better fit compared to 5% Manugel (Fig.3-4A). Therefore, the error between the curves also suggests that the diffusion coefficient of 2% Protanal is larger than 5% Manugel.

We hypothesize the error present in the system can be reduced even further by optimizing: (1) the flowrate and/or the Petri dish cap headspace to reduce the velocity at the surface of the water even further (2) improving the temperature control of the system and gas feed.

The system was then applied to formulations of alginate to determine their diffusion properties. Interestingly, different formulations of alginate seem to have a much more significant impact on the measured diffusivity coefficient than alginate concentration. This may suggest that more work needs to be done to measure the diffusivity than just calculating it using concentration or viscosity. Moreover, this finding stresses the importance of measuring the diffusion coefficient experimentally the exact factors influencing the value remain unclear.

The effect of diffusion on cell viability was quantified by live/dead staining and related to the Thiele modulus. The Thiele modulus refers to the rate of cellular oxygen consumption and was used to determine if an encapsulation device/system can meet this demand or if it is limited by mass transfer and diffusion. At high cell fractions (10 million MIN6 cells/mL) where the Thiele modulus is large ($\varphi >> \varphi_{crit}$), the cells become hypoxic because the oxygen cannot diffuse through the material fast enough to meet their demand, leading to necrosis and reduced effectiveness ($\eta << 1$). In the live/dead experiment (Fig. 3-8C and Fig. 3-8D), the oxygen within the material is not replenishing fast enough and decreases rapidly as a function of depth resulting in a very sharp live/dead cut-off ($\eta >> 1$). At such a high Thiele modulus like in Fig. 3-8D, the difference between the effectiveness factors for different materials becomes smaller (see Fig. 3-6). At a lower cell fraction (1.2 million cells/mL), differences between the materials become more obvious showing a significant difference between 2% protanal and 5% Manugel (see Fig. 3-8B).

The theoretical cell fractions in Fig. 3-7 suggest that the 2% protanal sample should have had adequate oxygenation at 1.2 million cells/mL which was not the case. This suggests that the model needs refinement when compared with the results in Fig. 3-8. Improved measure of the oxygen consumption rate or including Michaelis-Menten kinetics could overcome model limitations. Nevertheless, the results support the Thiele modulus hypothesis, where the difference in viability between samples is larger at low cell densities and much less obvious at high cell densities.

The data from Fig. 3-8D suggests that in a system with a large Thiele modulus ($\varphi >> \varphi_{crit}$), the oxygenation and cell viability are determined more by the cell fraction and oxygen consumption rate (cell type) than the choice of encapsulation material. At lower cell fractions where the effectiveness is closer to 1, the choice of material becomes more important.

Like MIN6 cells, islets are also regarded as an extremely aerobic cell type, natively they account for 10% of the blood flow in pancreas while only making up 1-2% of the cell mass [46]. At the cell fraction needed for a therapeutic implantable device (~600,000 IEQ for a 60kg person) [47] in a small device (<10mL), we hypothesize Fig. 3-8the therapeutic implantable device encapsulation material choice will have little impact on cell viability which will be low in all conditions.

Approximately a 375 mL microencapsulation device is needed to ensure viability of a therapeutic dose of islets that is properly oxygenated by diffusion Fig. 3-7B (600,000 islets at ~1600 islets/mL for 2% Protanal at $\eta = 0.9$). This size hurdle can be overcome using other oxygenation strategies, like adding more channels for flow, using an oxygen carrying fluid like blood, or even including oxygen-generating beads in the material [1,25]. In these scenarios, the choice of encapsulation material and its respective oxygen diffusion coefficient will become an increasingly important consideration as the system will start to behave more like what was observed in Fig. 3-8B with MIN6 cells at a lower cell density. In this case, a more diffusive material could mean having a smaller device with equivalent performance and the same therapeutic dose of insulin. In islet transplantation, a common approach is using an excess quantity of islets to compensate for early cell death as a result of poor oxygenation. If the cells were properly oxygenated ($\eta \geq 0.9$), the overall cell fraction and device size could be even smaller since it wouldn't need to compensate for early cell death due to improper oxygenation. In minimizing the device size and cell fraction, oxygen diffusion considerations and this approach could lead to a wider accessibility to this treatment since there will be more donated islets available for transplantation.

3.7 Conclusion

A simple method to measure the oxygen diffusion coefficient was developed for liquids and hydrogels commonly used for cellular encapsulation. The system was validated and measured the diffusion coefficient of water as $3.2x10^{-5} \pm 0.5x10^{-5}$ cm^2s^{-1} at 37°C which is within the range of what is currently documented in literature. The system measured the diffusion coefficient of three different formulations of hydrogels (2% Manugel, 2% Protanal, and 5% Manugel). The results of this work suggest that diffusivity is highly affected by alginate composition, a factor mentioned less often in numerical modeling work that use diffusivity values from literature. Moreover, measuring the oxygen diffusivity experimentally allows a more predictive approximation of Thiele and effectiveness factors which are useful dimensionless numbers for encapsulation device sizing and predicting trends is cellular viability.

3.8 Impact and Outlook

This work focused on a method to easily measure oxygen diffusion in different encapsulation materials. As fields like cell encapsulation and 3D cell culture continue to grow, and as islet transplantation becomes a more established clinical practice, the importance of oxygen transport to cells in hydrogels will become increasingly important. An accessible method to measure a critical parameter like the oxygen diffusion coefficient will be useful for many groups undertaking similar projects while using cell encapsulation or oxygen transport numerical modelling.

3.9 Acknowledgements

The authors gratefully acknowledge the funding that made this work possible, including the Stem Cell Network Fueling Biotechnology grant in collaboration with Aspect Biosystems led by

Timothy Kieffer at UBC. The work was also supported by funding from JDRF, Diabetes Canada, FRQNT, and NSERC Discovery (RGPIN-2018-06161 and RGPIN-2020-05877). I would like to acknowledge the funding from McGill University such as the Vadasz Scholar Award, and the Fonds de recherche du Québec – Nature et Technologies (FRQNT) for their support. I would like to acknowledge the help of Jonathan Brassard and Florent Lemaire for the help in making these experiments possible. I would also like to thank Berit Strand for the help in analyzing results, and Marco Pineda from the Yargeau Laboratory at McGill University for the help with equipment.

3.10 References

[1] S.A. Fernandez, K.S. Champion, L. Danielczak, M. Gasparrini, S. Paraskevas, R.L. Leask, C.A. Hoesli, Engineering Vascularized Islet Macroencapsulation Devices: An in vitro Platform to Study Oxygen Transport in Perfused Immobilized Pancreatic Beta Cell Cultures, Front. Bioeng. Biotechnol. 10 (2022). https://doi.org/10.3389/FBIOE.2022.884071.

[2] M. Neumann, T. Arnould, B.L. Su, Encapsulation of stem-cell derived β-cells: A promising approach for the treatment for type 1 diabetes mellitus, J. Colloid Interface Sci. 636 (2023) 90–102. https://doi.org/10.1016/J.JCIS.2022.12.123.

[3] M. Farina, J.F. Alexander, U. Thekkedath, M. Ferrari, A. Grattoni, Cell encapsulation: Overcoming barriers in cell transplantation in diabetes and beyond, Adv. Drug Deliv. Rev. 139 (2019) 92–115. https://doi.org/10.1016/J.ADDR.2018.04.018.

[4] K. Shah, Encapsulated stem cells for cancer therapy, Https://Doi.Org/10.4161/Biom.24278. 3 (2013). https://doi.org/10.4161/BIOM.24278.

[5] C.K. Colton, Oxygen supply to encapsulated therapeutic cells, Adv. Drug Deliv. Rev. 67–

68 (2014) 93–110. https://doi.org/10.1016/j.addr.2014.02.007.

[6] H. Komatsu, F. Kandeel, Y. Mullen, Impact of Oxygen on Pancreatic Islet Survival, Pancreas. 47 (2018) 533–543. https://doi.org/10.1097/MPA.0000000000001050.

[7] D.T. Bowers, W. Song, L.H. Wang, M. Ma, Engineering the vasculature for islet transplantation, Acta Biomater. 95 (2019) 131–151. https://doi.org/10.1016/J.ACTBIO.2019.05.051.

[8] T.M. Suszynski, E.S. Avgoustiniatos, K.K. Papas, Intraportal islet oxygenation, J. Diabetes Sci. Technol. 8 (2014) 575–580. https://doi.org/10.1177/1932296814525827.

[9] K. Verhoeff, B.A. Marfil-Garza, A.M.J. Shapiro, Update on islet cell transplantation, Curr. Opin. Organ Transplant. 26 (2021) 397–404. https://doi.org/10.1097/MOT.0000000000000891.

[10] A.M. James Shapiro, M. Pokrywczynska, C. Ricordi, Clinical pancreatic islet transplantation, Nat. Publ. Gr. (2016). https://doi.org/10.1038/nrendo.2016.178.

[11] E.D. Foster, N.D. Bridges, I.D. Feurer, T.L. Eggerman, L.G. Hunsicker, R. Alejandro, Improved Health-Related Quality of Life in a Phase 3 Islet Transplantation Trial in Type 1 Diabetes Complicated by Severe Hypoglycemia, Diabetes Care. (2018) dc171779. https://doi.org/10.2337/dc17-1779.

[12] L.C. Pullen, Islet cell transplantation hits a milestone, Am. J. Transplant. 21 (2021) 2625–2626. https://doi.org/10.1111/AJT.16039.

[13] T. Van Belle, M. Von Herrath, Immunosuppression in islet transplantation, J. Clin. Invest. 118 (2008) 1625–1628. https://doi.org/10.1172/JCI35639.

[14] E.D. Foster, N.D. Bridges, I.D. Feurer, T.L. Eggerman, L.G. Hunsicker, R. Alejandro, B. Begley, J. Cano, S. Carpentier, J. Hutchinson, C.P. Larsen, J. Moreno, M. Sears, N.A.

Turgeon, D. Webster, J.F. Markmann, P. Al-saden, X. Chen, A. Hecyk, X. Luo, M. Molitch, N. Monson, E. Stuart, A. Wallia, L. Wang, S. Wang, X. Zhang, C.W. Czarniecki, J.S. Goldstein, A. Priore, M.A. Robien, E. Schneider, G. Arreaza-Rubin, N. Green, D.L. Bigam, P. Campbell, P. Dinyari, T. Kin, N.M. Kneteman, J. Lyon, A. Malcolm, D. O'Gorman, C. Onderka, R. Owen, R. Pawlick, B. Richer, S. Rosichuk, D. Sarman, A. Schroeder, P.A. Senior, A.M.J. Shapiro, L. Toth, V. Toth, W. Zhai, K. Johnson, J. McElroy, A.M. Posselt, M. Ramos, T. Rojas, P.G. Stock, G. Szot, B. Barbaro, J. Martellotto, J. Oberholzer, M. Qi, Y. Wang, L. Bayman, K. Chaloner, W.R. Clarke, J.S. Dillon, C. Diltz, G.C. Doelle, D. Ecklund, D. Feddersen, C. Jasperson, D.-E. Lafontant, T. Neill-Hudson, D. Nollen, J. Qidwai, H. Riss, T. Schwieger, J. Willits, J. Yankey, A.C. Corrales, R. Faradji, T. Froud, A. Alvarez Gil, E. Herrada, L. Inverardi, N. Kenyon, A. Khan, E. Linetsky, E. Peixoto, C. Ricordi, M.H. Abdulla, A.N. Balamurugan, M.D. Bellin, M. Brandenburg, J. V. Harmon, B.J. Hering, R. Kandaswamy, G. Loganathan, K. Mueller, K.K. Papas, J. Pedersen, J.J. Wilhelm, J. Witson, C. Dalton-Bakes, H. Fu, M. Kamoun, J. Kearns, Y. Li, C. Liu, E. Luning-Prak, Y. Luo, E. Markmann, Z. Min, A. Naji, M. Palanjian, M.R. Rickels, R. Shlansky-Goldberg, K. Vivek, A.S. Ziaie, D.B. Kaufman, O. Korsgren, Improved Health-Related Quality of Life in a Phase 3 Islet Transplantation Trial in Type 1 Diabetes Complicated by Severe Hypoglycemia, Diabetes Care. 41 (2018) 1001–1008. https://doi.org/10.2337/DC17-1779.

[15] B.N. Moeun, S. Da Ling, M. Gasparrini, A.K. Rutman, S. Negi, S. Paraskevas, C.A. Hoesli, Islet encapsulation: A long-term treatment for type 1 diabetes, Elsevier, 2019. https://doi.org/10.1016/B978-0-12-801238-3.11135-3.

[16] G.A. Paredes Juárez, M. Spasojevic, M.M. Faas, P. Vos, Immunological and technical

considerations in application of alginate-based microencapsulation systems considerations in application of alginate-based microencapsulation systems., Front. Bioeng. Biotechnol. (2014). https://doi.org/10.3389/fbioe.2014.00026.

[17] C. Hoesli, R. Kiang, D. Mocinecová, M. Speck, D. Mošková, C. Donald-Hague, I. Lacík, T. Kieffer, J. Piret, Reversal of diabetes by βTC3 cells encapsulated in alginate beads generated by emulsion and internal gelation, J. Biomed. Mater. Res. B. Appl. Biomater. 100 (2012) 1017–1028. https://doi.org/10.1002/JBM.B.32667.

[18] M.A. Bochenek, O. Veiseh, A.J. Vegas, J.J. McGarrigle, M. Qi, E. Marchese, M. Omami, J.C. Doloff, J. Mendoza-Elias, M. Nourmohammadzadeh, A. Khan, C.C. Yeh, Y. Xing, D. Isa, S. Ghani, J. Li, C. Landry, A.R. Bader, K. Olejnik, M. Chen, J. Hollister-Lock, Y. Wang, D.L. Greiner, G.C. Weir, B.L. Strand, A.M.A. Rokstad, I. Lacik, R. Langer, D.G. Anderson, J. Oberholzer, Alginate encapsulation as long-term immune protection of allogeneic pancreatic islet cells transplanted into the omental bursa of macaques, Nat. Biomed. Eng. 2 (2018) 810–821. https://doi.org/10.1038/s41551-018-0275-1.

[19] B. Buder, M. Alexander, R. Krishnan, D.W. Chapman, J.R. Lakey, Encapsulated Islet Transplantation: Strategies and Clinical Trials, Immune Netw. 13 (2013) 235–239. https://doi.org/10.4110/IN.2013.13.6.235.

[20] T. Linn, J. Schmitz, I. Hauck-Schmalenberger, Y. Lai, R.G. Bretzel, H. Brandhorst, D. Brandhorst, Ischaemia is linked to inflammation and induction of angiogenesis in pancreatic islets, Clin. Exp. Immunol. 144 (2006) 179. https://doi.org/10.1111/J.1365-2249.2006.03066.X.

[21] F. Stephanie, D. Marc-André, B.-D. André, R. Jean, L. Richard, H. Corinne, Towards the fabrication of a 3D printed vascularized islet transplantation device for the treatment of

type 1 diabetes, Front. Bioeng. Biotechnol. 4 (2016). https://doi.org/10.3389/conf.fbioe.2016.01.01021.

[22] P. Buchwald, A local glucose-and oxygen concentration-based insulin secretion model for pancreatic islets, Theor. Biol. Med. Model. 8 (2011). https://doi.org/10.1186/1742-4682-8-20.

[23] A.S. Johnson, R.J. Fisher, G.C. Weir, C.K. Colton, Oxygen consumption and diffusion in assemblages of respiring spheres: Performance enhancement of a bioartificial pancreas, Chem. Eng. Sci. 64 (2009) 4470–4487. https://doi.org/10.1016/j.ces.2009.06.028.

[24] R. Cao, E. Avgoustiniatos, K. Papas, P. de Vos, J.R.T. Lakey, Mathematical predictions of oxygen availability in micro- and macro-encapsulated human and porcine pancreatic islets, J. Biomed. Mater. Res. - Part B Appl. Biomater. 108 (2020) 343–352. https://doi.org/10.1002/jbm.b.34393.

[25] J.P. Liang, R.P. Accolla, M. Soundirarajan, A. Emerson, M.M. Coronel, C.L. Stabler, Engineering a macroporous oxygen-generating scaffold for enhancing islet cell transplantation within an extrahepatic site, Acta Biomater. 130 (2021) 268–280. https://doi.org/10.1016/J.ACTBIO.2021.05.028.

[26] A. Al-Ani, D. Toms, D. Kondro, J. Thundathil, Y. Yuid, M. Ungrinid, Oxygenation in cell culture: Critical parameters for reproducibility are routinely not reported, (2018). https://doi.org/10.1371/journal.pone.0204269.

[27] Ü. Mehmetoğlu, S. Ateş, R. Berber, Oxygen diffusivity in calcium alginate gel beads containing Gluconobacter suboxydans, Artif. Cells. Blood Substit. Immobil. Biotechnol. 24 (1996) 91–106. https://doi.org/10.3109/10731199609118877.

[28] D. Cristea, S. Krishtul, P. Kuppusamy, L. Baruch, M. Machluf, A. Blank, New approach

to measuring oxygen diffusion and consumption in encapsulated living cells, based on electron spin resonance microscopy, Acta Biomater. 101 (2020) 384–394. https://doi.org/10.1016/J.ACTBIO.2019.10.032.

[29] L. Figueiredo, R. Pace, C. D'Arros, G. Réthoré, J. Guicheux, C. Le Visage, P. Weiss, Assessing glucose and oxygen diffusion in hydrogels for the rational design of 3D stem cell scaffolds in regenerative medicine, J. Tissue Eng. Regen. Med. 12 (2018) 1238–1246. https://doi.org/10.1002/TERM.2656.

[30] K. Bhunia, S.S. Sablani, J. Tang, B. Rasco, Non-invasive measurement of oxygen diffusion in model foods, Food Res. Int. 89 (2016) 161–168. https://doi.org/10.1016/J.FOODRES.2016.07.015.

[31] Y. Rharbi, A. Yekta, M.A. Winnik, A Method for Measuring Oxygen Diffusion and Oxygen Permeation in Polymer Films Based on Fluorescence Quenching, Anal. Chem. 71 (1999) 5045–5053. https://doi.org/10.1021/AC990193C.

[32] T. Fiedler, I. V. Belova, G.E. Murch, G. Poologasundarampillai, J.R. Jones, J.A. Roether, A.R. Boccaccini, A comparative study of oxygen diffusion in tissue engineering scaffolds, J. Mater. Sci. Mater. Med. 25 (2014) 2573–2578. https://doi.org/10.1007/S10856-014-5264-7.

[33] A.E. Al-Muftah, I.M. Abu-Reesh, Effects of internal mass transfer and product inhibition on a simulated immobilized enzyme-catalyzed reactor for lactose hydrolysis, Biochem. Eng. J. 23 (2005) 139–153. https://doi.org/10.1016/J.BEJ.2004.10.010.

[34] E.S. Avgoustiniatos, C.K. Colton, Effect of External Oxygen Mass Transfer Resistances on Viability of Immunoisolated Tissuea, Ann. N. Y. Acad. Sci. 831 (1997) 145–166. https://doi.org/10.1111/J.1749-6632.1997.TB52192.X.

[35] J.R.H. Ross, Mass and Heat Transfer Limitations and Other Aspects of the Use of Large-Scale Catalytic Reactors, Contemp. Catal. (2019) 187–213. https://doi.org/10.1016/B978-0-444-63474-0.00008-4.

[36] F.M. Pereira, S.C. Oliveira, Occurrence of dead core in catalytic particles containing immobilized enzymes: analysis for the Michaelis–Menten kinetics and assessment of numerical methods, Bioprocess Biosyst. Eng. 39 (2016) 1717–1727. https://doi.org/10.1007/S00449-016-1647-0.

[37] X. Liu, stage_file_maker, MATLAB Cent. File Exch. (2023). https://www.mathworks.com/matlabcentral/fileexchange/68849-stage_file_maker (accessed March 22, 2023).

[38] S. Preibisch, S. Saalfeld, P. Tomancak, Globally optimal stitching of tiled 3D microscopic image acquisitions, Bioinformatics. 25 (2009) 1463–1465. https://doi.org/10.1093/BIOINFORMATICS/BTP184.

[39] P. Buchwald, FEM-based oxygen consumption and cell viability models for avascular pancreatic islets, Theor. Biol. Med. Model. 6 (2009) 5. https://doi.org/10.1186/1742-4682-6-5.

[40] C.R. Wilke, P. Chang, Correlation of diffusion coefficients in dilute solutions, AIChE J. 1 (1955) 264–270. https://doi.org/10.1002/AIC.690010222.

[41] F. Noël, B. Mauroy, Interplay between optimal ventilation and gas transport in a model of the human lung, Front. Physiol. 10 (2019). https://doi.org/10.3389/FPHYS.2019.00488.

[42] W. Xing, M. Yin, Q. Lv, Y. Hu, C. Liu, J. Zhang, Oxygen Solubility, Diffusion Coefficient, and Solution Viscosity, Rotating Electrode Methods Oxyg. Reduct. Electrocatal. (2014) 1–31. https://doi.org/10.1016/B978-0-444-63278-4.00001-X.

[43] S. Arora, F. Potucek, Modelling of displacement washing of packed bed of fibers, Brazilian J. Chem. Eng. 26 (2009) 385–393. https://doi.org/10.1590/S0104-66322009000200016.

[44] I.A. Ganaie, S. Arora, V.K. Kukreja, Modelling and simulation of a packed bed of pulp fibers using mixed collocation method, Int. J. Differ. Equations. 2013 (2013). https://doi.org/10.1155/2013/875298.

[45] C. Androjna, J.E. Gatica, J.M. Belovich, K.A. Derwin, Oxygen diffusion through natural extracellular matrices: Implications for estimating “critical thickness” values in tendon tissue engineering, Tissue Eng. - Part A. 14 (2008) 559–569. https://doi.org/10.1089/TEA.2006.0361.

[46] H. Peiris, C.S. Bonder, P.T.H. Coates, D.J. Keating, C.F. Jessup, The β-Cell/EC Axis: How Do Islet Cells Talk to Each Other?, Diabetes. 63 (2014) 3–11. https://doi.org/10.2337/DB13-0617.

[47] S. Lablanche, S. Borot, A. Wojtusciszyn, K. Skaare, A. Penfornis, P. Malvezzi, L. Badet, C. Thivolet, E. Morelon, F. Buron, E. Renard, I. Tauveron, O. Villard, M. Munch, S. Sommacal, L. Clouaire, M. Jacquet, L. Gonsaud, C. Camillo-Brault, C. Colin, J.L. Bosson, D. Bosco, T. Berney, L. Kessler, P.Y. Benhamou, Ten-year outcomes of islet transplantation in patients with type 1 diabetes: Data from the Swiss-French GRAGIL network, Am. J. Transplant. 21 (2021) 3725–3733. https://doi.org/10.1111/AJT.16637.

4 Chapter 4: Discussion and Future Work

4.1 Discussion

The main objectives of this thesis were to develop a simpler way to measure the oxygen diffusivity of hydrogels, and to use experimental diffusion coefficients to refine a numerical model and predict cellular behaviour. The underlying goal of this project is to improve numerical models used for islet transplantation to help expedite the delivery of a type 1 diabetes treatment making use of encapsulated islets by providing robust inputs for design modelling.

In this work, a method to experimentally determine the oxygen diffusivity of liquids and hydrogels was developed and only requires a simple gas flow system, a temperature-controlled box, a Petri dish, a simple 3D-printed cap (see Appendix 7.3), and an oxygen sensing fixed needle probe (OXPT500; Pyroscience). Many of these items are available in most laboratories working with cell culture, as most incubators are temperature and humidity controlled, while using gases like CO_2 to control pH levels in cell media. By blending 3 gas types (nitrogen, air, CO_2) in a controlled fashion with rotameters, humidifying the gas through an Erlenmeyer filled with water, and passing the gas in the headspace of the glass Petri dish with 3D printed cap, the surface boundary condition can be controlled. Changes in the system can be recorded at a discrete point using the oxygen sensing probe.

The system was verified using computational fluid dynamics to ensure that the gas flow at the surface boundary does not introduce too much advection into the system, while ensuring it is fast enough to quickly change and maintain the headspace of the Petri dish at a desired concentration. The computational fluid dynamics suggests that at the chosen nominal gas flowrate of 130 mL/min, the Peclet number (ratio of advective to diffusive transport) is still below 1 at the center axis where the probe is located. Since the Peclet number is below 1, the system is

diffusion dominant and the advective term of the general convection equation can be neglected. This improves the accuracy of the system since the experiment isolates only for the diffusion coefficient term.

The system was validated by experimentally measuring the oxygen diffusion coefficient of water at 37°C which is approximately 2.9-3.3x10^{-5} cm^2s^{-1} [18,72,79–81]. In this work, it was taken as 3.1x10^{-5} cm^2s^{-1}. When measuring reverse osmosis (RO) water at 37°C, the system developed in this work predicts the oxygen diffusivity to be 3.2x10^{-5} cm^2s^{-1} ± 0.5x10^{-5} cm^2s^{-1}, this value corresponds to an absolute percent error of about 3.3%. The average measured diffusion value is within the range of current literature. Moreover, the error (±0.5x10^{-5} cm^2s^{-1}) can be justified as some sources have reported RO water to have a diffusivity as low as 2.6x10^{-5} cm^2s^{-1} [81], and as high as 3.83x10^{-5} cm^2s^{-1} [92] at 37°C. This demonstrates the completion of one of the major objectives of this work, which was to develop a simple way to accurately measure the oxygen diffusion.

The system was used to find the oxygen diffusion of 2 types of alginate hydrogels (10/60 LF Protanal and Manugel GHB at 2% w/v), and to test the effect of concentration by comparing 2% w/v Manugel to 5% w/v Manugel. Unsurprisingly, the most viscous of all the gels was the least diffusive with a diffusion coefficient of 1.1x10^{-5} cm^2s^{-1} ± 0.4x10^{-5} cm^2s^{-1}, its visual higher viscosity is attributable to the higher mass percentage of 5% w/v compared to 2% w/v during solution preparation. The most viscous gel being the least diffusive is consistent with the Stokes-Einstein relationship between viscosity and diffusivity [87], which states that increased viscosity is inversely correlated with the diffusion coefficient.

The error between the numerical model and experimental data, albeit small, overshoots the data initially and undershoots the data as the oxygen concentration approaches 0%. This trend is consistent with an error resulting from increased advection where the Pe may go above 1. The error for 5% Manugel (least diffusive hydrogel) was the highest compared to 2% Protanal (most diffusive hydrogel) which had the lowest error. Since the Pe number is influenced by the diffusion coefficient, the error profiles are consistent with the findings, the least diffusive material would have more error, especially if the Pe number is close to 1.

The molecular analysis of both Manugel and Protanal was performed both in powder format and post autoclaving (see Appendix 7.1). Autoclaved samples were subjected to a liquid 30 cycle and were prepared in 100mL batches. Afterwards, the samples were dialyzed and lyophilized to allow for analysis in a solid format. Unsurprisingly, the molecular weight for both types decreased after autoclaving due to the breakdown of molecular chains at higher temperatures (~120°C). The M/G ratio is slightly lower for Manugel compared to Protanal indicating that there might be more internal crosslinking in the Manugel samples, but the difference may not be large enough to explain the large difference in oxygen diffusivity. In general, the molecular chain properties for Protanal and Manugel are similar (as shown in Table 3 in the Appendix 7.1). Despite the difference being small, Manugel has more G, GG, and GGG chain content which again could also suggest that the material is more cross-linked. The molecular weights of both alginates as well as the polydispersity (M_w/M_n) is also fairly similar. Further investigation could determine exactly which property is causing the significant difference in oxygen diffusion or to determine how sensitive the diffusion coefficient is to small differences in molecular G content.

MIN6 cells were then encapsulated into the 3 tested materials to assess the effect of the hydrogel on cell viability. Moreover, the Thiele modulus and effectiveness factor were calculated and

compared to the experimental viability results. The Thiele modulus is a dimensionless number that is the ratio of reaction rate to the rate of diffusion. From a cellular perspective, it is the rate at which cells consume oxygen compared to how fast oxygen can diffuse into the system. At high values of the Thiele modulus, cells are consuming oxygen faster than it can be supplied making the system less effective and limited by the rate of oxygen mass transfer. The effectiveness factor is a dimensionless number between 0 and 1 that describes how well the cells are being oxygenated. At an effectiveness factor close to or equal to 1, there are no mass transfer limitations. From a cellular perspective, there is an abundance of oxygen available to meet the demands of the cells. Conversely, at low values of the effectiveness factor (close to 0), there is not enough oxygen in the system to meet the demand of the cells, this could be due to the cells being very aerobic or simply having a very large cell fraction. The effectiveness factor is non-linear: it is constant at 1 when the Thiele modulus is below the critical Thiele modulus and begins to descend to 0 asymptotically (see Fig. 3-7). Theoretically, at larger values of the Thiele modulus, differences in the effectiveness factor will become less pronounced due to the non-linear nature of the curve beyond the critical Thiele modulus. Since the cell fraction is linearly related to the Thiele modulus, the difference in effectiveness factor would become less obvious at higher cell fractions when $\varphi >> \varphi_{crit}$ and more obvious at lower cell fractions.

At lower MIN6 cell fractions (1.2 million cells per mL), there was a significant difference between 5% Manugel and 2% Protanal, while at higher concentrations (10 million cells per mL) there was no significance among groups (see Fig. 3-8). This result is consistent with the effectiveness factor plot and theory. If the cell fraction were to decrease even further from 1.2 million cells / mL we would expect this trend to continue, the difference among the groups

would likely become more drastic until the viability for each alginate type reaches 100%. When the viability reaches 100%, this would correspond to an effectiveness factor of 1.

Table 2 Thiele modulus and effectiveness factor at 1.2 million cells/mL and 10 million cells/mL for MIN6

Hydrogel	**1.2 million MIN6 cells/mL**		**10 million MIN6 cells/mL**	
	Thiele Modulus (φ)	Effectiveness factor (η)	Thiele Modulus (φ)	Effectiveness factor (η)
2% Manugel	1.7	0.83	7.6	0.19
2% Protanal	1.3	1	6.6	0.21
5% Manugel	2.0	0.72	8.6	0.16

Table 2 shows the exact effectiveness factor and Thiele modulus for all hydrogels calculated at the cell fractions used for the cell work in Fig 3-8. Unsurprisingly, at 10 million cells/mL the difference in effectiveness between groups is very marginal due to the high Thiele modulus which is much larger than φ_{crit}. At 1.2 million cells/mL, the difference between groups is now quite significant, 2% Protanal supposedly has an effectiveness of 1 while 5% Manugel can theoretically only achieve and effectiveness of 0.7 at the same cell fraction.

Interestingly, the effectiveness factors and/or their spacing from each other very closely resemble the dimensionless viability value determined in Fig 3-8. At 10 million cells/mL, the groups have a very close theoretical effectiveness factor of ~0.2, in Fig 3-8D, all the dimensionless viability values were also ~0.2. At a lower cell fraction (1.2 million cells/mL), the theoretical effectiveness factor did not exactly match the values seen in Fig 3-8C, however the difference between the groups (the spacing) aligns fairly well with the results in Table 2. For example, the

difference between 2% Protanal and 5% Manugel was approximately ~0.3 in both the dimensionless viability in Fig 3-8C and in Table 2. Similarly, the difference between 2% Protanal and 2% Manugel was ~0.2 in both Table 2 and Fig 3-8C.

Additional research is needed to evaluate if this trend is coincidental or to see if the effectiveness factor is this closely related to dimensionless viability. Currently, the effectiveness factor and Thiele modulus offer a general understanding of the trends in cellular behaviour and its non-linearity at different cell fractions. This relationship is based on a ratio of rate of oxygen consumption and mass transfer limitations. To better understand if there is a quantitative relationship between effectiveness factor and dimensionless viability, more cell fractions could be tested and compared. If such a quantitative relationship does exist, it is likely that the model is less susceptible to errors at higher cell fractions. The difference between 9.5 million cells/mL and 10 million cells/mL does not change the results that much (effectiveness of 2% Protanal would go from 0.21 to 0.24). While at lower cell fractions near φ_{crit} (1.2 million cells/mL), a difference of 500,000 cells per mL can completely change the effectiveness factor values (see Fig. 3-6 near φ_{crit}). Nevertheless, the effectiveness factor provides a wealth of information both a low and high cell fractions for cellular behaviour and viability. While there is not currently enough information about how well the effectiveness factor can predict the exact value of cell viability, it is possible that the two are connected quantitatively, but further investigation is needed to confirm this.

Another potential source of error is the use of a 0^{th} order model instead of a 1^{st} order model. A 1^{st} order model would provide better numerical accuracy since more terms were accounted for, such as the Michaelis-Menten coefficient (K_m). One caveat to this is that current literature only has a good estimate for the Michaelis-Menten coefficient for islets, and the value would have to be

measured for MIN6. Nevertheless, for the purpose of this work, the 0^{th} order kinetics are sufficient for determining trends in cellular viability and the assumptions required to use it hold true (primarily that $C_s >> K_m$). Since the surface oxygen tension changes as a function of cell fraction and geometry (see Appendix 7.2), it is possible that at a high enough cell fraction a 0^{th} order model no longer applies. Nevertheless, the 0^{th} order assumption was preferred over using 1^{st} order kinetics because the exact value for K_m for MIN6 is unknown and the surface oxygen tension large. Despite the exact value for K_m being unknown for MIN6, it is reasonable to assume it is in the same order of magnitude as that for islets (K_m of ~ 0.44 mmHg [19,39,68]) which is sufficiently low compared to normal surface concentrations (C_s) in this work. Even in the worst case with 10 million MIN6 cells in the most diffusive material (2% pronatal), surface oxygen levels would never be lower than 0.03 $molm^{-3}$ (~25 mmHg) (See Appendix 7.2) which is still much larger than the K_m of islets (0.44 mmHg).

Based on the results shown in Fig. 3-7 and Fig. 3-8, the choice of encapsulation material is important provided the cell fraction allows for proper oxygenation. If the cell fraction is too high, all types of encapsulation materials will produce poor results as shown in Fig. 3-8. However, at a low enough cell fraction, the choice in encapsulation material could be very important for medical device design. A medical device using Protanal may be able to theoretically hold almost 2,000 more islets /mL than the Manugel formulations while still achieving the same oxygenation (see Fig. 3-7). In practice, this value may be lower however the trend is the same, a more diffusive material will produce higher cell viability. Currently, medical devices are aiming to be as small as possible while still delivering a therapeutic dose of insulin. Moreover, many devices will add an excess of islets to compensate for early cell death which is attributed to the lack of vasculature and oxygenation. Choosing the correct encapsulation material allows for a medical

device to be smaller all the while achieving good oxygenation. A cell fraction like ~2,000 islets / mL (presented as 2% Protanal in Fig. 3-6) is too small for a medical device since a therapeutic dose would be on the scale of 100,000 islets, this would correspond to a medical device approximately 300 cm^3 in size for 600,000 islets. Other alternatives exist to improve the oxygenation, such as the incorporation of oxygen generating beads, the use of blood flow, promoting angiogenesis to grow vasculature, or even internal perfusable channels to include advective oxygen transport. In these scenarios, the effectiveness factor will likely be closer to 1 due to the improved oxygenation from the additional design change. Since all of these devices would still be using encapsulation, the choice of material then becomes important the same way it would be at lower cell fractions without oxygen generation, vasculature, etc. Choosing the correct encapsulation material with better oxygen diffusion performance could translate to having a device with islets that are more densely packed while still being properly oxygenated and functional. Therefore, the ability to measure the oxygen diffusion of different hydrogels could help miniaturize islet encapsulation devices while still delivering a therapeutic dose of insulin.

The current system does have limitations. For instance, the use of gas flow as a way of controlling the boundary oxygen levels will always introduce a small amount of error resulting from advection. If the gas flowrate is too small, then the boundary will not be properly held at the desired oxygen concentration. In the results, our system appears to work well at 130 mL/min but we are approaching the edge of failure as some materials like 5% Manugel were starting to show larger amounts of error between the experimental data and the model (see Fig. 3-4A) likely due to the smaller oxygen diffusion coefficient. Therefore, for much less diffusive materials such as a much more dense hydrogel, the system may not be able to measure without introducing too

much error from advection. This limitation can be overcome by optimizing the flowrate for the application, deciding an acceptable gas flowrate to properly control the boundary condition while also not introducing too much error. Another limitation is that the system has only currently been tested on liquids and internally gelled alginates. Many methods use external gelation as the primary encapsulation method. The system can likely be used for externally gelled alginate but there would need to be an extra step where gelling solution is added directly in the Petri dish around the probe and swapped out later for cell media. Finally, when using internal gelation like in the manuscript, it is important to wait for the alginate to swell and for the oxygen levels to stabilize before running the experiment. Often times, the oxygen levels would temporarily decrease in the gel during the swelling phase likely due to the production of CO_2 as a by-product of the GDL reaction. The system has to settle back to equilibrium at 21% oxygen before running the diffusion experiment. This process can take a few h, at which point the system may have changed slightly due to evaporation or other factors like swelling. This limitation can be overcome by running an identical sample in parallel made from the same stock solution solely to measure the geometry after the oxygen has been restored. However, it is currently not possible to get the exact geometry of the slab being measured without stopping the experiment.

4.2 Future Work

Future work for this system includes measuring more alginate gels including those produced using external gelation. Demonstrating the systems abilities for this type of gelation method would increase the usefulness of the method for many other groups interested in oxygen diffusion. Further investigation into determining which material property is affecting the diffusion coefficient is needed, some examples could be doing rheology to get a numerical value to compare the complex viscosities of the different gelled formulations. Using islets instead of

MIN6 for live/dead staining will also provide a lot of information into which encapsulation material results in the best islet oxygenation. While MIN6 cells are a useful for modelling islet behaviour, using actual islets can provide more relevant information such as experimental cell fractions that result in proper oxygenation for different encapsulation materials. Despite islets being the better cellular model, the same trend with diffusivity and cell fraction noticed with MIN6 cells will likely occur with islets. Another interesting next step would be incorporating oxygen producing beads in the hydrogel to evaluate the effects of an oxygen source on cellular behaviour, the Thiele modulus, and the oxygen diffusion coefficient.

5 Chapter 5: Conclusion and Summary

The primary objective of this work was to explore a more accessible method to measure the oxygen diffusion coefficient for hydrogels (Fig. 3-1 to Fig 3-5). The second objective was to use the method to experimentally measure the oxygen diffusion coefficient for common cell encapsulation materials and use it to predict cellular behaviour using a numerical model (Fig. 3-6 to Fig. 3-8). Both of these objectives were met through the course of this manuscript as shown in key figures.

A simple method to measure the oxygen diffusion coefficient was developed and validated using computational fluid dynamics and a standard (reverse osmosis water at 37°C), the well-known oxygen diffusion coefficient of water was compared to experimental output. The system was then used to measure 3 different formulations of alginate, a very common hydrogel used for cell encapsulation. After obtaining experimental oxygen diffusion coefficients for these alginate formulations, MIN6 cells were encapsulated in the alginate at different cell fractions to explore the relationship between diffusion and cell viability. Ultimately the relationship between the diffusion coefficient and cell viability follows trends similar to those seen with the effectiveness factor and Thiele modulus. At higher cell fractions, the viability between groups with different oxygen diffusivity was less noticeable compared to at low cell fractions.

This work demonstrates the importance of measuring the oxygen diffusion coefficient since it can change depending on the alginate formulation. For other labs that are also working with cell encapsulation, the oxygen diffusion coefficient will become increasingly important as cell therapies continue to be developed and researched. Moreover, as islet transplantation continues to become an established clinical practice, islet encapsulation and methods for improved

oxygenation will also become increasingly important. The method developed in this thesis is capable of measuring the oxygen diffusivity in many materials relevant to islet transplantation and was created with the goal of expediting a treatment to chronic illnesses like type 1 diabetes.

6 References

[1] M. Mobasseri, M. Shirmohammadi, T. Amiri, N. Vahed, H.H. Fard, M. Ghojazadeh, Prevalence and incidence of type 1 diabetes in the world: A systematic review and meta-analysis, Heal. Promot. Perspect. 10 (2020) 98–115. https://doi.org/10.34172/hpp.2020.18.

[2] A.J. Delli, Å. Lernmark, Autoimmune (Type 1) Diabetes, in: Autoimmune Dis. Fifth Ed., Elsevier Inc., 2013: pp. 575–586. https://doi.org/10.1016/B978-0-12-384929-8.00041-1.

[3] P.E. MacDonald, P. Rorsman, Oscillations, Intercellular Coupling, and Insulin Secretion in Pancreatic β Cells, PLoS Biol. 4 (2006) e49. https://doi.org/10.1371/journal.pbio.0040049.

[4] R.B. Vernon, A. Preisinger, M.D. Gooden, L.A. D'Amico, B.B. Yue, P.L. Bollyky, C.S. Kuhr, T.R. Hefty, G.T. Nepom, J.A. Gebe, Reversal of diabetes in mice with a bioengineered islet implant incorporating a type I collagen hydrogel and sustained release of vascular endothelial growth factor, Cell Transplant. 21 (2012) 2099–2110. https://doi.org/10.3727/096368912X636786.

[5] S.J. Prowse, K.J. Lafferty, C.J. Simeonovic, M. Agostino, K.M. Bowen, E.J. Steele, The reversal of diabetes by pancreatic islet transplantation, Diabetes. 31 (1982) 30–38. https://doi.org/10.2337/diab.31.4.s30.

[6] E.D. Foster, N.D. Bridges, I.D. Feurer, T.L. Eggerman, L.G. Hunsicker, R. Alejandro, Improved Health-Related Quality of Life in a Phase 3 Islet Transplantation Trial in Type 1 Diabetes Complicated by Severe Hypoglycemia, Diabetes Care. (2018) dc171779. https://doi.org/10.2337/dc17-1779.

[7] G. Salomone, MUHC designated first provincial establishment for islet cell transplants for patients with type 1 diabetes , McGill Univ. Heal. Cent. (2022). https://rimuhc.ca/-/muhc-

designated-first-provincial-establishment-for-islet-cell-transplants-for-patients-with-type-1-diabetes?redirect=%2Fwhats-new-ri-muhc (accessed March 12, 2023).

[8] H. Komatsu, D. Kang, L. Medrano, A. Barriga, D. Mendez, J. Rawson, K. Omori, K. Ferreri, Y.C. Tai, F. Kandeel, Y. Mullen, Isolated human islets require hyperoxia to maintain islet mass, metabolism, and function, Biochem. Biophys. Res. Commun. 470 (2016) 534–538. https://doi.org/10.1016/j.bbrc.2016.01.110.

[9] D.T. Bowers, W. Song, L.H. Wang, M. Ma, Engineering the vasculature for islet transplantation, Acta Biomater. 95 (2019) 131–151. https://doi.org/10.1016/j.actbio.2019.05.051.

[10] G.A. Paredes Juárez, M. Spasojevic, M.M. Faas, P. Vos, Immunological and technical considerations in application of alginate-based microencapsulation systems considerations in application of alginate-based microencapsulation systems., Front. Bioeng. Biotechnol. (2014). https://doi.org/10.3389/fbioe.2014.00026.

[11] B.N. Moeun, S. Da Ling, M. Gasparrini, A.K. Rutman, S. Negi, S. Paraskevas, C.A. Hoesli, Islet encapsulation: A long-term treatment for type 1 diabetes, Elsevier, 2019. https://doi.org/10.1016/B978-0-12-801238-3.11135-3.

[12] K.K. Papas, E.S. Avgoustiniatos, T.M. Suszynski, Effect of oxygen supply on the size of implantable islet-containing encapsulation devices, Panminerva Med. 58 (2016) 72–77. https://arizona.pure.elsevier.com/en/publications/effect-of-oxygen-supply-on-the-size-of-implantable-islet-containi (accessed February 26, 2021).

[13] L. Figueiredo, R. Pace, C. D'Arros, G. Réthoré, J. Guicheux, C. Le Visage, P. Weiss, Assessing glucose and oxygen diffusion in hydrogels for the rational design of 3D stem cell scaffolds in regenerative medicine, J. Tissue Eng. Regen. Med. 12 (2018) 1238–1246.

https://doi.org/10.1002/TERM.2656.

[14] K. Bhunia, S.S. Sablani, J. Tang, B. Rasco, Non-invasive measurement of oxygen diffusion in model foods, Food Res. Int. 89 (2016) 161–168. https://doi.org/10.1016/J.FOODRES.2016.07.015.

[15] Ü. Mehmetoğlu, S. Ateş, R. Berber, Oxygen diffusivity in calcium alginate gel beads containing Gluconobacter suboxydans, Artif. Cells. Blood Substit. Immobil. Biotechnol. 24 (1996) 91–106. https://doi.org/10.3109/10731199609118877.

[16] C. Magliaro, G. Mattei, F. Iacoangeli, A. Corti, V. Piemonte, A. Ahluwalia, Oxygen Consumption Characteristics in 3D Constructs Depend on Cell Density, Front. Bioeng. Biotechnol. 7 (2019) 251. https://doi.org/10.3389/fbioe.2019.00251.

[17] F.M. Docherty, H.A. Russ, Cell-cell interactions driving differentiation of adult pancreatic stem cells, in: Encycl. Tissue Eng. Regen. Med., Elsevier, 2019: pp. 367–374. https://doi.org/10.1016/B978-0-12-801238-3.65615-5.

[18] P. Buchwald, FEM-based oxygen consumption and cell viability models for avascular pancreatic islets, Theor. Biol. Med. Model. 6 (2009) 5. https://doi.org/10.1186/1742-4682-6-5.

[19] P. Buchwald, A local glucose-and oxygen concentration-based insulin secretion model for pancreatic islets, Theor. Biol. Med. Model. 8 (2011). https://doi.org/10.1186/1742-4682-8-20.

[20] H.J. Woerle, J.E. Gerich, Glucose Physiology, Normal, Encycl. Endocr. Dis. (2004) 263–270. https://doi.org/10.1016/B0-12-475570-4/00616-8.

[21] D.P. Zaharieva, K. Turksoy, S.M. McGaugh, R. Pooni, T. Vienneau, T. Ly, M.C. Riddell, Lag Time Remains with Newer Real-Time Continuous Glucose Monitoring Technology

during Aerobic Exercise in Adults Living with Type 1 Diabetes, Diabetes Technol. Ther. 21 (2019) 313–321. https://doi.org/10.1089/dia.2018.0364.

[22] E. Latres, D.A. Finan, J.L. Greenstein, A. Kowalski, T.J. Kieffer, Navigating Two Roads to Glucose Normalization in Diabetes: Automated Insulin Delivery Devices and Cell Therapy, Cell Metab. 29 (2019) 545–563. https://doi.org/10.1016/j.cmet.2019.02.007.

[23] M.M. Hafiz, R.N. Faradji, T. Froud, A. Pileggi, D.A. Baidal, P. Cure, G. Ponte, R. Poggioli, A. Cornejo, S. Messinger, C. Ricordi, R. Alejandro, Immunosuppression and procedure-related complications in 26 patients with type 1 diabetes mellitus receiving allogeneic islet cell transplantation, Transplantation. 80 (2005) 1718–1728. https://doi.org/10.1097/01.tp.0000187881.97068.77.

[24] M.W. Lauria, A. Ribeiro-Oliveira, Diabetes and other endocrine-metabolic abnormalities in the long-term follow-up of pancreas transplantation, Clin. Diabetes Endocrinol. 2 (2016). https://doi.org/10.1186/s40842-016-0032-x.

[25] K.K. Papas, H. De Leon, T.M. Suszynski, R.C. Johnson, Oxygenation strategies for encapsulated islet and beta cell transplants, Adv. Drug Deliv. Rev. 139 (2019) 139–156. https://doi.org/10.1016/j.addr.2019.05.002.

[26] W.M. Kühtreiberc, L.T. Ho, A. Kamireddy, J.A.W. Yacoub, D.W. Scharp, Islet isolation from human pancreas with extended cold ischemia time, in: Transplant. Proc., Elsevier, 2010: pp. 2027–2031. https://doi.org/10.1016/j.transproceed.2010.05.099.

[27] C.K. Colton, Oxygen supply to encapsulated therapeutic cells, Adv. Drug Deliv. Rev. 67–68 (2014) 93–110. https://doi.org/10.1016/j.addr.2014.02.007.

[28] L.R. Iuamoto, A. Meyer, E. Chaib, L.A.C. D'Albuquerque, Review of experimental attempts of islet allotransplantation in rodents: Parameters involved and viability of the

procedure, World J. Gastroenterol. 20 (2014) 13512–13520. https://doi.org/10.3748/wjg.v20.i37.13512.

[29] E.P. Brandon, M.J. Scott, M.C. Zimmerman, K.A. D'Amour, Pluripotent Stem Cell–Derived Islet Replacement Therapy for Diabetes, in: Second Gener. Cell Gene-Based Ther., Elsevier, 2020: pp. 157–181. https://doi.org/10.1016/b978-0-12-812034-7.00006-6.

[30] T. Watanabe, T. Okitsu, F. Ozawa, S. Nagata, H. Matsunari, H. Nagashima, M. Nagaya, H. Teramae, S. Takeuchi, Millimeter-thick xenoislet-laden fibers as retrievable transplants mitigate foreign body reactions for long-term glycemic control in diabetic mice, Biomaterials. 255 (2020) 120162. https://doi.org/10.1016/j.biomaterials.2020.120162.

[31] O. Korsgren, Islet encapsulation: Physiological possibilities and limitations, Diabetes. 66 (2017) 1748–1754. https://doi.org/10.2337/db17-0065.

[32] M.A. Bochenek, O. Veiseh, A.J. Vegas, J.J. McGarrigle, M. Qi, E. Marchese, M. Omami, J.C. Doloff, J. Mendoza-Elias, M. Nourmohammadzadeh, A. Khan, C.C. Yeh, Y. Xing, D. Isa, S. Ghani, J. Li, C. Landry, A.R. Bader, K. Olejnik, M. Chen, J. Hollister-Lock, Y. Wang, D.L. Greiner, G.C. Weir, B.L. Strand, A.M.A. Rokstad, I. Lacik, R. Langer, D.G. Anderson, J. Oberholzer, Alginate encapsulation as long-term immune protection of allogeneic pancreatic islet cells transplanted into the omental bursa of macaques, Nat. Biomed. Eng. 2 (2018) 810–821. https://doi.org/10.1038/s41551-018-0275-1.

[33] N. Li, Y. Zhang, Z. Xiu, Y. Wang, L. Chen, S. Wang, S. Li, X. Guo, X. Ma, The preservation of islet with alginate encapsulation in the process of transportation, Biotechnol. Appl. Biochem. 62 (2015) 530–536. https://doi.org/10.1002/bab.1295.

[34] J.D. Weaver, D.M. Headen, M.M. Coronel, M.D. Hunckler, H. Shirwan, A.J. García, Synthetic poly(ethylene glycol)-based microfluidic islet encapsulation reduces graft

volume for delivery to highly vascularized and retrievable transplant site, Am. J. Transplant. 19 (2019) 1315–1327. https://doi.org/10.1111/ajt.15168.

[35] D. Jacobs-Tulleneers-Thevissen, M. Chintinne, Z. Ling, P. Gillard, L. Schoonjans, G. Delvaux, B.L. Strand, F. Gorus, B. Keymeulen, D. Pipeleers, Sustained function of alginate-encapsulated human islet cell implants in the peritoneal cavity of mice leading to a pilot study in a type 1 diabetic patient, Diabetologia. 56 (2013) 1605–1614. https://doi.org/10.1007/s00125-013-2906-0.

[36] F. Luzi, D. Puglia, L. Torre, Natural fiber biodegradable composites and nanocomposites: A biomedical application, in: Biomass, Biopolym. Mater. Bioenergy Constr. Biomed. Other Ind. Appl., Elsevier, 2019: pp. 179–201. https://doi.org/10.1016/B978-0-08-102426-3.00010-2.

[37] B. Buder, M. Alexander, R. Krishnan, D.W. Chapman, J.R. Lakey, Encapsulated Islet Transplantation: Strategies and Clinical Trials, Immune Netw. 13 (2013) 235–239. https://doi.org/10.4110/IN.2013.13.6.235.

[38] H. Komatsu, F. Kandeel, Y. Mullen, Impact of Oxygen on Pancreatic Islet Survival, Pancreas. 47 (2018) 533–543. https://doi.org/10.1097/MPA.0000000000001050.

[39] A.S. Johnson, R.J. Fisher, G.C. Weir, C.K. Colton, Oxygen consumption and diffusion in assemblages of respiring spheres: Performance enhancement of a bioartificial pancreas, Chem. Eng. Sci. 64 (2009) 4470–4487. https://doi.org/10.1016/j.ces.2009.06.028.

[40] C. Mas-Bargues, J. Sanz-Ros, A. Román-Domínguez, M. Inglés, L. Gimeno-Mallench, M. El Alami, J. Viña-Almunia, J. Gambini, J. Viña, C. Borrás, Relevance of oxygen concentration in stem cell culture for regenerative medicine, Int. J. Mol. Sci. 20 (2019). https://doi.org/10.3390/ijms20051195.

[41] V. Delaune, T. Berney, S. Lacotte, C. Toso, Intraportal islet transplantation: the impact of the liver microenvironment, Transpl. Int. 30 (2017) 227–238. https://doi.org/10.1111/tri.12919.

[42] G.R. Cunha, L. Baskin, Use of sub-renal capsule transplantation in developmental biology, Differentiation. 91 (2016) 4–9. https://doi.org/10.1016/j.diff.2015.10.007.

[43] H. Onoe, T. Okitsu, A. Itou, S. Takeuchi, LONG-TERM IMPLANTATION OF PRIMARY ISLET CELL-ENCAPSULATING HYDROGEL MICROFIBERS IN DIABETIC MICE, n.d.

[44] C. Schmidt, Pancreatic islets find a new transplant home in the omentum, Nat. Biotechnol. 35 (2017) 8. https://doi.org/10.1038/nbt0117-8.

[45] C.K. Colton, Challenges in the Development of Immunoisolation Devices, in: Princ. Tissue Eng. Fourth Ed., Elsevier Inc., 2013: pp. 543–562. https://doi.org/10.1016/B978-0-12-398358-9.00028-8.

[46] M. Ohtas, D. Nelson, J. Nelson, M.D. Meglassonq, M. Erecitika, Oxygen and Temperature Dependence of Stimulated Insulin Secretion in Isolated Rat Islets of Langerhans", 1990. https://doi.org/10.1016/S0021-9258(18)38196-1.

[47] H. Komatsu, C. Cook, C.H. Wang, L. Medrano, H. Lin, F. Kandeel, Y.C. Tai, Y. Mullen, Oxygen environment and islet size are the primary limiting factors of isolated pancreatic islet survival, PLoS One. 12 (2017). https://doi.org/10.1371/journal.pone.0183780.

[48] G.C. Weir, Islet encapsulation: advances and obstacles, Diabetologia. 56 (2013) 1458–1461. https://doi.org/10.1007/S00125-013-2921-1.

[49] A. Rabinovitch, W.L. Suarez-Pinzon, Cytokines and their roles in pancreatic islet beta-cell destruction and insulin-dependent diabetes mellitus., Biochem. Pharmacol. 55 (1998)

1139–1149. https://doi.org/10.1016/s0006-2952(97)00492-9.

[50] M. de Groot, P.P. Keizer, B.J. de Haan, T.A. Schuurs, H.G. Leuvenink, R. van Schilfgaarde, P. de Vos, Microcapsules and their ability to protect islets against cytokine-mediated dysfunction, Transplant. Proc. 33 (2001) 1711–1712. https://doi.org/10.1016/s0041-1345(00)02653-1.

[51] V. Vaithilingam, B.E. Tuch, Islet transplantation and encapsulation: an update on recent developments., Rev. Diabet. Stud. 8 (2011) 51–67. https://doi.org/10.1900/RDS.2011.8.51.

[52] D. Goswami, D.A. Domingo-Lopez, N.A. Ward, J.R. Millman, G.P. Duffy, E.B. Dolan, E.T. Roche, Design Considerations for Macroencapsulation Devices for Stem Cell Derived Islets for the Treatment of Type 1 Diabetes., Adv. Sci. (Weinheim, Baden-Wurttemberg, Ger. 8 (2021) e2100820. https://doi.org/10.1002/advs.202100820.

[53] U. Barkai, A. Rotem, P. de Vos, Survival of encapsulated islets: More than a membrane story., World J. Transplant. 6 (2016) 69–90. https://doi.org/10.5500/wjt.v6.i1.69.

[54] S.K. Tam, S. Bilodeau, J. Dusseault, G. Langlois, J.-P. Hallé, L.H. Yahia, Biocompatibility and physicochemical characteristics of alginate–polycation microcapsules, Acta Biomater. 7 (2011) 1683–1692. https://doi.org/https://doi.org/10.1016/j.actbio.2010.12.006.

[55] L.A. Llacua, B.J. de Haan, P. de Vos, Laminin and collagen IV inclusion in immunoisolating microcapsules reduces cytokine-mediated cell death in human pancreatic islets., J. Tissue Eng. Regen. Med. 12 (2018) 460–467. https://doi.org/10.1002/term.2472.

[56] S. Song, G. Faleo, R. Yeung, R. Kant, A.M. Posselt, T.A. Desai, Q. Tang, S. Roy, Silicon

nanopore membrane (SNM) for islet encapsulation and immunoisolation under convective transport, Sci. Rep. 6 (2016) 23679. https://doi.org/10.1038/srep23679.

[57] Q. Zhang, C. Gonelle-Gispert, Y. Li, Z. Geng, S. Gerber-Lemaire, Y. Wang, L. Buhler, Islet Encapsulation: New Developments for the Treatment of Type 1 Diabetes., Front. Immunol. 13 (2022) 869984. https://doi.org/10.3389/fimmu.2022.869984.

[58] P. Soon-Shiong, E. Feldman, R. Nelson, R. Heintz, Q. Yao, Z. Yao, T. Zheng, N. Merideth, G. Skjak-Braek, T. Espevik, Long-term reversal of diabetes by the injection of immunoprotected islets., Proc. Natl. Acad. Sci. 90 (1993) 5843–5847. https://doi.org/10.1073/pnas.90.12.5843.

[59] C. Hoesli, R. Kiang, D. Mocinecová, M. Speck, D. Mošková, C. Donald-Hague, I. Lacík, T. Kieffer, J. Piret, Reversal of diabetes by βTC3 cells encapsulated in alginate beads generated by emulsion and internal gelation, J. Biomed. Mater. Res. B. Appl. Biomater. 100 (2012) 1017–1028. https://doi.org/10.1002/JBM.B.32667.

[60] V. Kozlovskaya, O. Zavgorodnya, E. Kharlampieva, Encapsulation and Surface Engineering of Pancreatic Islets: Advances and Challenges, in: C. Lin (Ed.), IntechOpen, Rijeka, 2012: p. Ch. 1. https://doi.org/10.5772/33951.

[61] P. de Vos, H.A. Lazarjani, D. Poncelet, M.M. Faas, Polymers in cell encapsulation from an enveloped cell perspective., Adv. Drug Deliv. Rev. 67–68 (2014) 15–34. https://doi.org/10.1016/j.addr.2013.11.005.

[62] L. Robles, R. Storrs, M. Lamb, M. Alexander, J.R.T. Lakey, Current status of islet encapsulation., Cell Transplant. 23 (2014) 1321–1348. https://doi.org/10.3727/096368913X670949.

[63] S. Bose, L.R. Volpatti, D. Thiono, V. Yesilyurt, C. McGladrigan, Y. Tang, A. Facklam, A.

Wang, S. Jhunjhunwala, O. Veiseh, J. Hollister-Lock, C. Bhattacharya, G.C. Weir, D.L. Greiner, R. Langer, D.G. Anderson, A retrievable implant for the long-term encapsulation and survival of therapeutic xenogeneic cells, Nat. Biomed. Eng. 4 (2020) 814–826. https://doi.org/10.1038/s41551-020-0538-5.

[64] D.T. Bowers, W. Song, L.H. Wang, M. Ma, Engineering the vasculature for islet transplantation, Acta Biomater. 95 (2019) 131–151. https://doi.org/10.1016/J.ACTBIO.2019.05.051.

[65] L.-H. Wang, A.U. Ernst, D. An, A.K. Datta, B. Epel, M. Kotecha, M. Ma, A bioinspired scaffold for rapid oxygenation of cell encapsulation systems., Nat. Commun. 12 (2021) 5846. https://doi.org/10.1038/s41467-021-26126-w.

[66] K.E. Dionne, C.K. Colton, M.L. Yarmush, Effect of oxygen on isolated pancreatic tissue, ASAIO Trans. 35 (1989) 739–741. https://doi.org/10.1097/00002480-198907000-00185.

[67] R.J. Fleischaker, A.J. Sinskey, Oxygen demand and supply in cell culture, Eur. J. Appl. Microbiol. Biotechnol. 12 (1981) 193–197. https://doi.org/10.1007/BF00499486.

[68] E.S. Avgoustiniatos, C.K. Colton, Effect of External Oxygen Mass Transfer Resistances on Viability of Immunoisolated Tissuea, Ann. N. Y. Acad. Sci. 831 (1997) 145–166. https://doi.org/10.1111/J.1749-6632.1997.TB52192.X.

[69] T.W. Secomb, R. Hsu, E.Y.H. Park, M.W. Dewhirst, Green's function methods for analysis of oxygen delivery to tissue by microvascular networks, Ann. Biomed. Eng. 32 (2004) 1519–1529. https://doi.org/10.1114/B:ABME.0000049036.08817.44.

[70] R. Cao, E. Avgoustiniatos, K. Papas, P. de Vos, J.R.T. Lakey, Mathematical predictions of oxygen availability in micro- and macro-encapsulated human and porcine pancreatic islets, J. Biomed. Mater. Res. - Part B Appl. Biomater. 108 (2020) 343–352.

https://doi.org/10.1002/jbm.b.34393.

[71] E.S. Avgoustiniatos, K.E. Dionne, D.F. Wilson, M.L. Yarmush, C.K. Colton, Measurements of the effective diffusion coefficient of oxygen in pancreatic islets, Ind. Eng. Chem. Res. 46 (2007) 6157–6163. https://doi.org/10.1021/ie070662y.

[72] A. Al-Ani, D. Toms, D. Kondro, J. Thundathil, Y. Yuid, M. Ungrinid, Oxygenation in cell culture: Critical parameters for reproducibility are routinely not reported, (2018). https://doi.org/10.1371/journal.pone.0204269.

[73] H.R. Lee, S.M. Jung, S. Yoon, W.H. Yoon, T.H. Park, S. Kim, H.W. Shin, D.S. Hwang, S. Jung, Immobilization of planktonic algal spores by inkjet printing, Sci. Rep. 9 (2019). https://doi.org/10.1038/S41598-019-48776-Z.

[74] E.S. Chan, T.K. Lim, W.P. Voo, R. Pogaku, B.T. Tey, Z. Zhang, Effect of formulation of alginate beads on their mechanical behavior and stiffness, Particuology. 9 (2011) 228–234. https://doi.org/10.1016/J.PARTIC.2010.12.002.

[75] P.E. Ramos, P. Silva, M.M. Alario, L.M. Pastrana, J.A. Teixeira, M.A. Cerqueira, A.A. Vicente, Effect of alginate molecular weight and M/G ratio in beads properties foreseeing the protection of probiotics, Food Hydrocoll. 77 (2018) 8–16. https://doi.org/10.1016/J.FOODHYD.2017.08.031.

[76] Ü. Mehmetoğlu, S. Ateş, R. Berber, Oxygen diffusivity in calcium alginate gel beads containing Gluconobacter suboxydans, Artif. Cells. Blood Substit. Immobil. Biotechnol. 24 (1996) 91–106. https://doi.org/10.3109/10731199609118877.

[77] A.C. Hulst, H.J.H. Hens, R.M. Buitelaar, J. Tramper, Determination of the effective diffusion coefficient of oxygen in gel materials in relation to gel concentration, Biotechnol. Tech. 3 (1989) 199–204. https://doi.org/10.1007/BF01875620.

[78] H. Hiemstra, L. Dijkhuizen, W. Harder, Diffusion of oxygen in alginate gels related to the kinetics of methanol oxidation by immobilized Hansenula polymorpha cells, Eur. J. Appl. Microbiol. Biotechnol. 18 (1983) 189–196. https://doi.org/10.1007/BF00501507.

[79] C.R. Wilke, P. Chang, Correlation of diffusion coefficients in dilute solutions, AIChE J. 1 (1955) 264–270. https://doi.org/10.1002/AIC.690010222.

[80] F. Noël, B. Mauroy, Interplay between optimal ventilation and gas transport in a model of the human lung, Front. Physiol. 10 (2019). https://doi.org/10.3389/FPHYS.2019.00488.

[81] W. Xing, M. Yin, Q. Lv, Y. Hu, C. Liu, J. Zhang, Oxygen Solubility, Diffusion Coefficient, and Solution Viscosity, Rotating Electrode Methods Oxyg. Reduct. Electrocatal. (2014) 1–31. https://doi.org/10.1016/B978-0-444-63278-4.00001-X.

[82] C. Hu, W. Lu, A. Mata, K. Nishinari, Y. Fang, Ions-induced gelation of alginate: Mechanisms and applications, Int. J. Biol. Macromol. 177 (2021) 578–588. https://doi.org/10.1016/J.IJBIOMAC.2021.02.086.

[83] L.W. Chan, H.Y. Lee, P.W.S. Heng, Mechanisms of external and internal gelation and their impact on the functions of alginate as a coat and delivery system, Carbohydr. Polym. 63 (2006) 176–187. https://doi.org/10.1016/J.CARBPOL.2005.07.033.

[84] E.A. Growney Kalaf, R. Flores, J.G. Bledsoe, S.A. Sell, Characterization of slow-gelling alginate hydrogels for intervertebral disc tissue-engineering applications, Mater. Sci. Eng. C. 63 (2016) 198–210. https://doi.org/10.1016/J.MSEC.2016.02.067.

[85] C. Maxwell, A. Soltisz, W. Rich, A. Choi, M. Reilly, K. Swindle-Reilly, Alginate Hydrogels as Injectable Drug Delivery Vehicles for Optic Neuropathy Treatment, 2021. https://doi.org/10.21203/rs.3.rs-391900/v1.

[86] C.A. Hoesli, R.L.J. Kiang, K. Raghuram, R.G. Pedroza, K.E. Markwick, A.M.R.

Colantuoni, J.M. Piret, Mammalian Cell Encapsulation in Alginate Beads Using a Simple Stirred Vessel, JoVE (Journal Vis. Exp. 2017 (2017) e55280. https://doi.org/10.3791/55280.

[87] W.M. Deen, Analysis of transport phenomena, (1998).

[88] D. Cristea, S. Krishtul, P. Kuppusamy, L. Baruch, M. Machluf, A. Blank, New approach to measuring oxygen diffusion and consumption in encapsulated living cells, based on electron spin resonance microscopy, Acta Biomater. 101 (2020) 384–394. https://doi.org/10.1016/J.ACTBIO.2019.10.032.

[89] T. Fiedler, I. V. Belova, G.E. Murch, G. Poologasundarampillai, J.R. Jones, J.A. Roether, A.R. Boccaccini, A comparative study of oxygen diffusion in tissue engineering scaffolds, J. Mater. Sci. Mater. Med. 25 (2014) 2573–2578. https://doi.org/10.1007/S10856-014-5264-7.

[90] A. Venâncio, J.A. Teixeira, Characterization of sugar diffusion coefficients in alginate membranes, Biotechnol. Tech. 11 (1997) 183–186. https://doi.org/10.1023/A:1018457631368.

[91] G.F. Itamunoala, Effective Diffusion Coefficients in Calcium Alginate Gel, Biotechnol. Prog. 3 (1987) 115–120. https://doi.org/10.1002/BTPR.5420030209.

[92] C. Androjna, J.E. Gatica, J.M. Belovich, K.A. Derwin, Oxygen diffusion through natural extracellular matrices: Implications for estimating “critical thickness” values in tendon tissue engineering, Tissue Eng. - Part A. 14 (2008) 559–569. https://doi.org/10.1089/TEA.2006.0361.

7 Appendix

7.1 Alginate molecular properties data

Table 3 Alginate molecular analysis

Alginate	Molecular Weight			M/G Ratio	Mannuronic Acid (M) / Guluronic Acid (G) Chain Analysis								
	M_w (kDa)	M_n (kDa)	M_w/M_n		F_G	F_M	F_{GG}	$F_{GM, MG}$	F_{MM}	$F_{GGM, MGG}$	F_{MGM}	F_{GGG}	$N_{G>1}$
Manugel GHB (powder)	176	73	2.4	0.47	0.68	0.32	0.57	0.11	0.21	0.041	0.071	0.53	15
Autoclaved Manugel GHB (2% w/v)	90	43	2.1										
Protanal 10/60 LF (powder)	143	64	2.2	0.49	0.67	0.33	0.55	0.11	0.22	0.039	0.078	0.52	15
Autoclaved Protanal 10/60 LF (2% w/v)	82	41	2.0										

Note: Autoclaved alginate was dialyzed and lyophilized to be returned into solid format before analysis. Alginate was autoclaved in a Liquid 30 cycle in volumes of 100mL.

7.2 Relationship between surface concentration and cell fraction used for calculating the Thiele modulus

The oxygen tension at the surface of the alginate which is below a small layer of media could vary from the oxygen tension at the surface of the media.

A 1-D model following the geometry in Fig 3-1D was developed. In the media portion (total length: 1.5mm), the diffusivity was assumed to be that of water at 37°C (3.1×10^{-5} $cm^2 s^{-1}$). In the hydrogel, the effective diffusivity (D_{eff}) was calculated using a weighted average of the cell fraction (the x variable), the oxygen diffusivity of tissue (D_{tissue}), and the experimental oxygen diffusivity of the hydrogel in question (2% Manugel, 2% Protanal, or 5% Manugel) referred to as D_{alg}. The oxygen diffusivity of tissue was taken as 1.24×10^{-5} $cm^2 s^{-1}$ [18,39]

$$D_{eff} = (1 - X)D_{alg} + (X)D_{tissue}$$

Choosing either the OCR for islets or MIN6, a relationship between the cell fraction and surface oxygen tension can be developed for a known geometry.

Note that to convert the unit "cells per mL" to IEQ for islets, a single cell was assumed as a sphere with a diameter of 10μm, and an islet was assumed to have a diameter of 150μm. Therefore, we assume there is ~3375 cells in a single islet equivalent (IEQ).

Note that 0.44 mmHg corresponds to about 6×10^{-4} $molm^{-3}$, this is the Michaelis-Menten coefficient of islets.

The relationships are as follows:

Islets (OCR = 0.034 molm^{-3}s^{-1})

2% Manugel (D_{alg} =1.5x10^{-5}cm^{2}s^{-1})

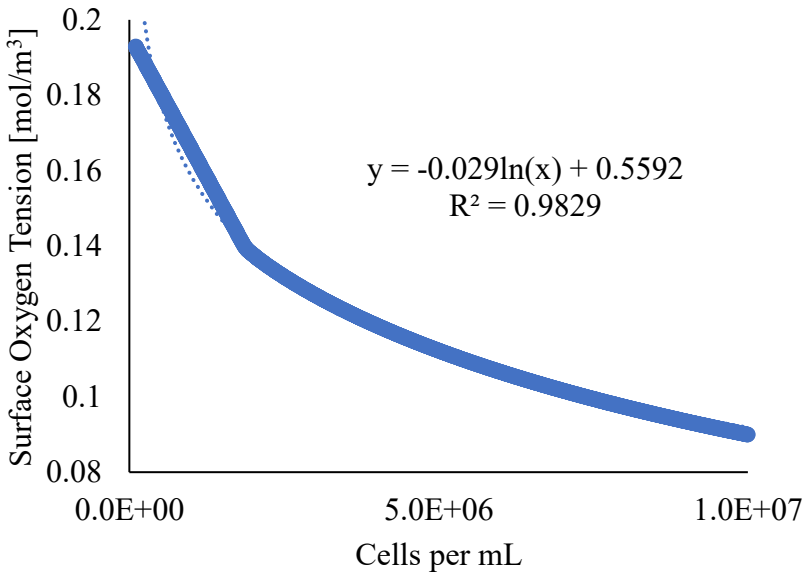

2% Protanal (D_{alg} = 2.7x10^{-5}cm^{2}s^{-1})

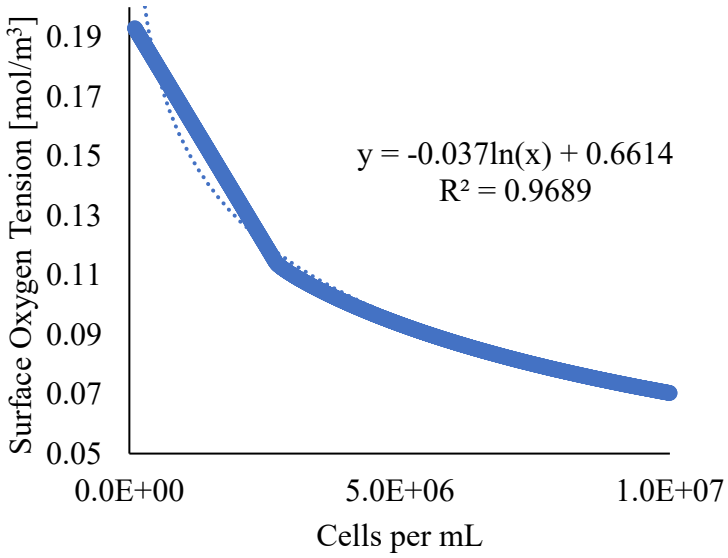

5% Manugel (D_{alg} = 1.1x10^{-5}cm^{2}s^{-1})

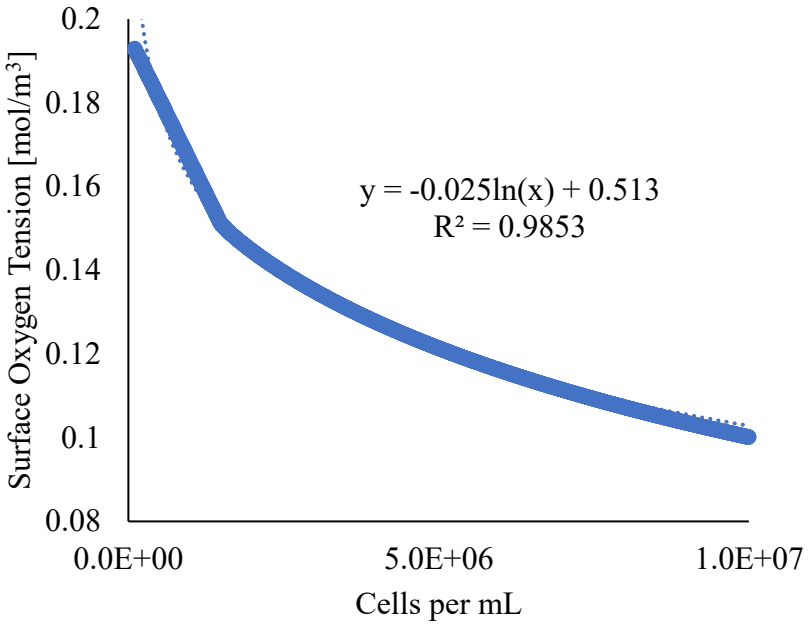

MIN6 Cell line (OCR = 0.129 molm^{-3}s^{-1})

2% Manugel (D_{alg} =1.5x10^{-5}cm^{2}s^{-1})

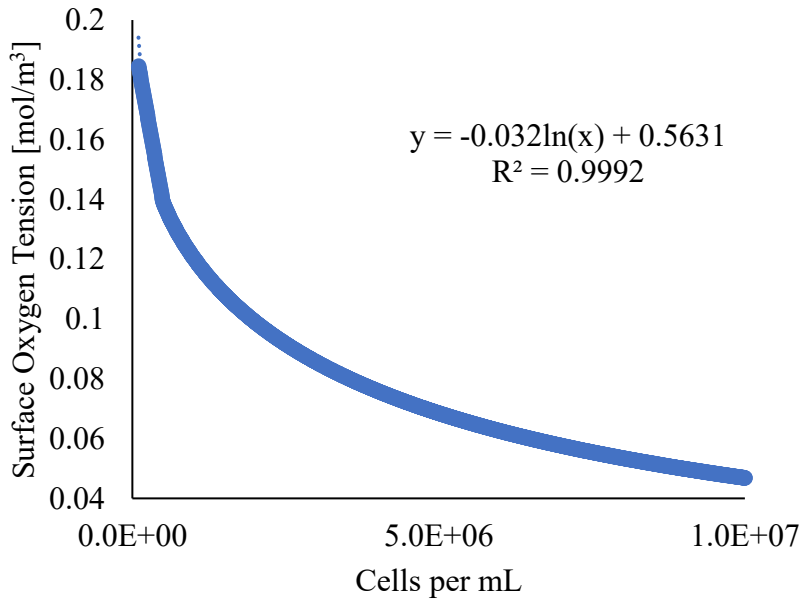

2% Protanal (D_{alg} = 2.7x10^{-5}cm^{2}s^{-1})

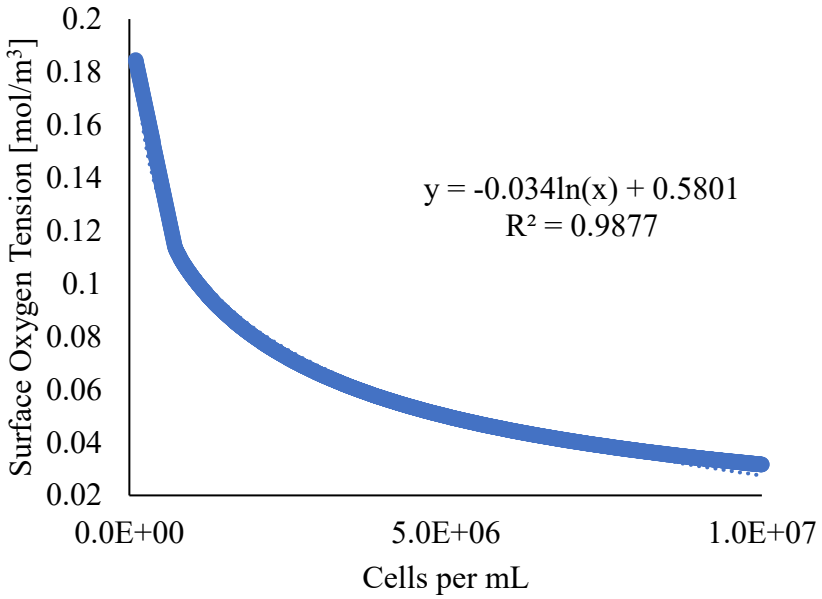

5% Manugel (D_{alg} = 1.1x10^{-5}cm^{2}s^{-1})

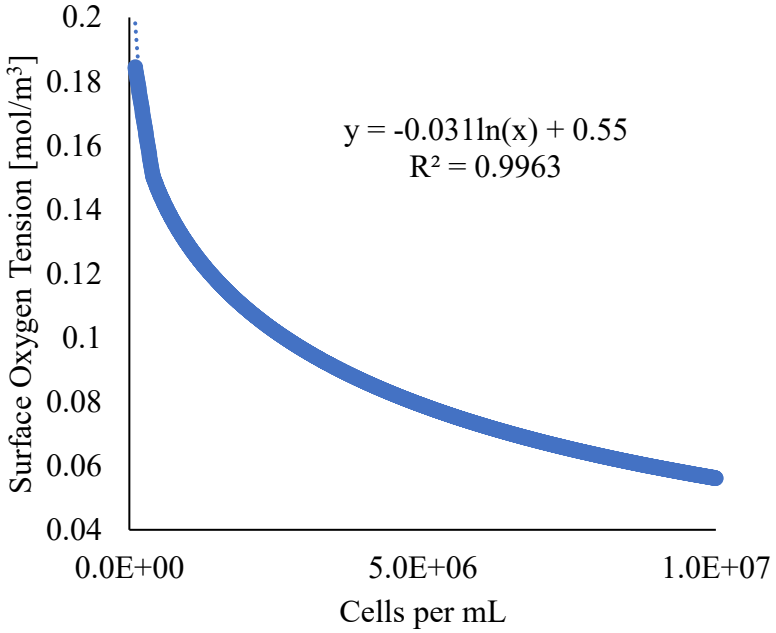

7.3 Technical Diagram of gas flow cap used in diffusion sensing setup

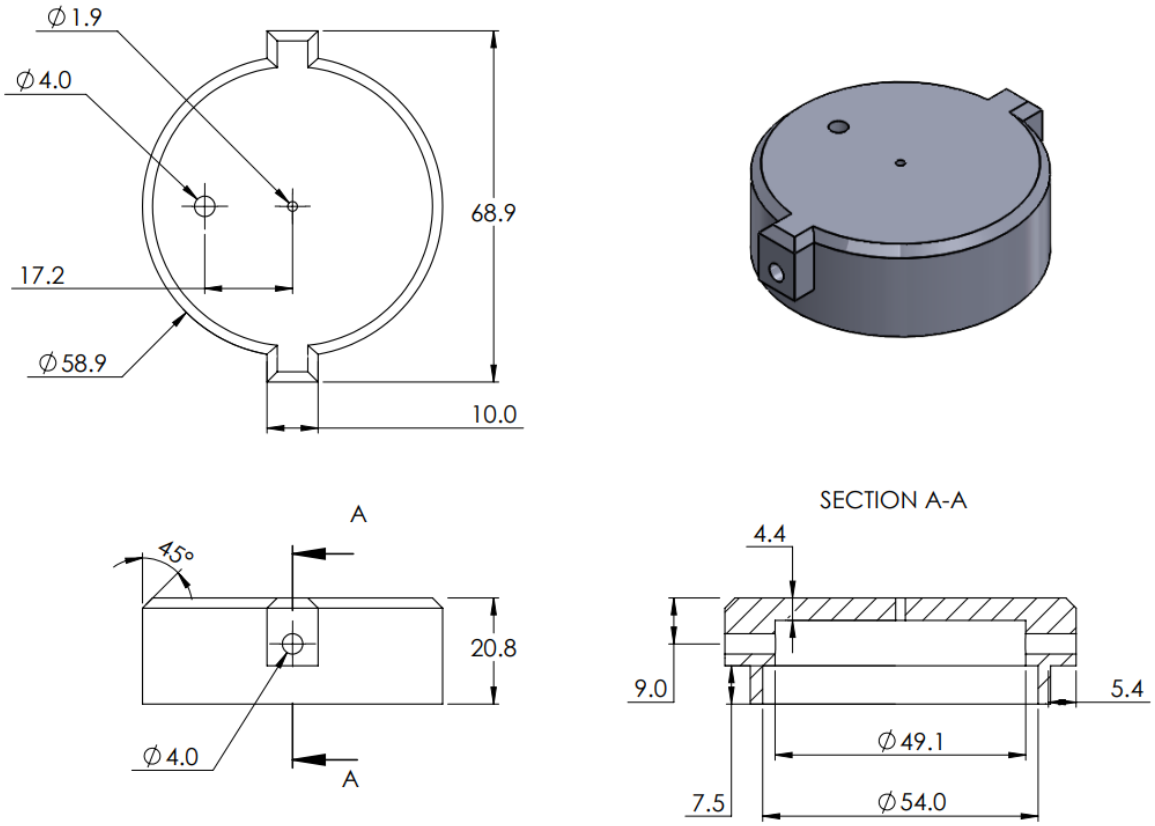

Units: millimeters (mm)

Note: The STL file will be provided with publication and/or upon request.

Barbed tube hose fittings are attached to both ends; they can be manually forced through when hose fitting has an M4 thread. A luer lock to hose thread can be attached to the top in the same manor. Between all fittings, small 4mm o-rings were used to create a better seal. The luer lock connection is sealed with a plastic male luer lock fixture. Assembly pictures are shown below: